

Global Biogeochemical Cycles®

RESEARCH ARTICLE

10.1029/2022GB007470

Timur Cinay and Diana Dumit contributed equally to this work.

Key Points:

- Secondary nitrite and pH maxima emerge in the oxygen deficient zone's upper anoxic core, overlaying a distinct tertiary nitrite maximum
- Anammox is the dominant mechanism for bioavailable nitrogen loss, and its relative rate is dependent on organic matter composition
- Denitrification of nitrite is the primary driver of the pH increase in the uppermost anoxic layers

Supporting Information:

Supporting Information may be found in the online version of this article.

Correspondence to:

T. Cinay and A. R. Babbin,
tcinay@mit.edu;
babbin@mit.edu

Citation:

Cinay, T., Dumit, D., Woosley, R. J., Boles, E. L., Kwiecinski, J. V., Mullen, S., et al. (2022). Coincident biogenic nitrite and pH maxima arise in the upper anoxic layer in the Eastern Tropical North Pacific. *Global Biogeochemical Cycles*, 36, e2022GB007470. <https://doi.org/10.1029/2022GB007470>

Received 22 MAY 2022

Accepted 5 DEC 2022

Author Contributions:

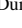






Conceptualization: Timur Cinay, Diana Dumit, Ryan J. Woosley, Andrew R. Babbin

Data curation: Timur Cinay, Diana Dumit, Ryan J. Woosley, Elisabeth L. Boles, Jarek V. Kwiecinski, Susan Mullen, Tyler J. Tamasi, Martin J. Wolf, Colette L. Kelly, Nicole M. Travis, Karen L. Casciotti, Andrew R. Babbin

© 2022. The Authors.

This is an open access article under the terms of the [Creative Commons Attribution-NonCommercial-NoDerivs License](#), which permits use and distribution in any medium, provided the original work is properly cited, the use is non-commercial and no modifications or adaptations are made.

Coincident Biogenic Nitrite and pH Maxima Arise in the Upper Anoxic Layer in the Eastern Tropical North Pacific

Timur Cinay¹ , Diana Dumit¹, Ryan J. Woosley^{1,2} , Elisabeth L. Boles^{1,3} , Jarek V. Kwiecinski^{1,4} , Susan Mullen^{1,5}, Tyler J. Tamasi¹, Martin J. Wolf^{1,6}, Colette L. Kelly⁷ , Nicole M. Travis⁷, Karen L. Casciotti⁷ , and Andrew R. Babbin¹ 

¹Department of Earth, Atmospheric and Planetary Sciences, Massachusetts Institute of Technology, Cambridge, MA, USA, ²Center for Global Change Science, Massachusetts Institute of Technology, Cambridge, MA, USA, ³Now at Department of Civil and Environmental Engineering, Stanford University, Stanford, CA, USA, ⁴Now at Division of Geological and Planetary Sciences, California Institute of Technology, Pasadena, CA, USA, ⁵Now at Department of Earth and Planetary Science, University of California, Berkeley, Berkeley, CA, USA, ⁶Now at Center for Environmental Law and Policy, Yale University, New Haven, CT, USA, ⁷Department of Earth System Science, Stanford University, Stanford, CA, USA

Abstract The Eastern Tropical North Pacific (ETNP), like the other marine oxygen deficient zones (ODZs), is characterized by an anoxic water column, nitrite accumulation at the anoxic core, and fixed nitrogen loss via nitrite reduction to N₂O and N₂ gases. Here, we constrain the relative contribution of biogeochemical processes to observable features such as the secondary nitrite maximum (SNM) and local pH maximum by simultaneous measurement of inorganic nitrogen and carbon species. High-resolution sampling within the top 1 km of the water column reveals consistent chemical features previously unobserved in the region, including a tertiary nitrite maximum. Dissolved inorganic carbon measurements show that pH increases with depth at the top of the ODZ, peaking at the potential density of the SNM at $\sigma_{\theta} = 26.15 \pm 0.06$ (1 s.d.). We developed a novel method to determine the relative contributions of anaerobic ammonium oxidation (anammox), denitrification, nitrite oxidation, dissimilatory nitrate reduction to nitrite, and calcium carbonate dissolution to the nitrite cycling in the anoxic ODZ core. The calculated relative contributions of each reaction are slightly sensitive to the assumed C:N:P ratio and the carbon oxidation state of the organic matter sinking through the ODZ. Furthermore, we identify the source of the pH increase at the top of ODZ as the net consumption of protons via nitrite reduction to N₂ by the denitrification process. The increase in pH due to denitrification impacts the buffering effect of calcite and aragonite dissolving in the ETNP.

1. Introduction

Marine oxygen deficient zones (ODZs) play a significant role in the global nitrogen cycle by removing 30%–50% of fixed nitrogen in the ocean, even though they comprise less than 0.1% of the ocean's volume (Brandes & Devol, 2002; Codispoti et al., 2001; DeVries et al., 2013; Gruber & Sarmiento, 1997; Karstensen et al., 2008). The Eastern Tropical North Pacific (ETNP) off Mexico and Central America is one of the three largest permanent ODZs (Kwiecinski & Babbin, 2021; Paulmier & Ruiz-Pino, 2009). The ETNP is characterized by highly productive coastal regions due to nutrient supply by the coastal upwelling (López-Sandoval et al., 2009; Stramma et al., 2010) and a large region of low-oxygen water column overlaid by predominantly oligotrophic surface ocean (Fuchsman, Palevsky, et al., 2019; Pennington et al., 2006). Below a well-mixed surface layer, oxygen concentrations decrease to levels as low as 10 nmol L⁻¹ (Morrison et al., 1998; Revsbech et al., 2009; Thamdrup et al., 2012; Tiano et al., 2014), corresponding to aerobic subsistence concentrations at which anaerobic metabolism can coexist with or dominate over aerobic respiration (Zakem & Follows, 2017).

Nitrite (NO₂⁻) is a central dissolved inorganic nitrogen (DIN) compound in the ODZ nitrogen cycle because it is a product or reactant for denitrification, anammox, and recycling of nitrate via dissimilatory nitrate reduction to nitrite (DNRN) and nitrite oxidation (Figure 1). A nitrate deficit and a similar magnitude excess of dissolved dinitrogen gas (N₂) concentrations in the ETNP imply the reduction of nitrite in the ODZ and consequential removal of the DIN (Chang et al., 2012; Fuchsman et al., 2018). Removal of biologically available DIN in ODZs is typically performed by either a heterotrophic denitrification process or autotrophic anaerobic ammonium oxidation (anammox) reaction (Babbin et al., 2014; Bristow et al., 2016; Ward, 2013). The proportion of nitrogen loss via denitrification and anammox, respectively, in the anoxic water column and the complexity of the complementary metabolisms that support them remain unresolved, particularly when considering the ODZ not as a uniform

Formal analysis: Timur Cinay, Diana Dumit
Funding acquisition: Karen L. Casciotti, Andrew R. Babbin
Investigation: Timur Cinay, Diana Dumit, Ryan J. Woosley, Elisabeth L. Boles, Jarek V. Kwiecinski, Susan Mullen, Tyler J. Tamasi, Martin J. Wolf, Colette L. Kelly, Nicole M. Travis, Karen L. Casciotti, Andrew R. Babbin
Methodology: Timur Cinay, Diana Dumit, Ryan J. Woosley, Elisabeth L. Boles, Jarek V. Kwiecinski, Susan Mullen, Tyler J. Tamasi, Martin J. Wolf, Colette L. Kelly, Nicole M. Travis, Karen L. Casciotti, Andrew R. Babbin
Project Administration: Ryan J. Woosley, Karen L. Casciotti, Andrew R. Babbin
Supervision: Ryan J. Woosley, Karen L. Casciotti, Andrew R. Babbin
Visualization: Timur Cinay
Writing – original draft: Timur Cinay, Andrew R. Babbin
Writing – review & editing: Timur Cinay, Diana Dumit, Ryan J. Woosley, Elisabeth L. Boles, Jarek V. Kwiecinski, Susan Mullen, Tyler J. Tamasi, Martin J. Wolf, Colette L. Kelly, Nicole M. Travis, Karen L. Casciotti, Andrew R. Babbin

system but as a complex combination of multiple isopycnal layers and water masses. While some studies suggest that, on a whole, anammox is the dominant production pathway for N_2 in the ODZ (Babbin et al., 2017; Kalvelage et al., 2013), others report that denitrification exceeds anammox in anoxic environments (Dalsgaard et al., 2012; Ward et al., 2009). Since denitrification and DNRN generate ammonium used in anammox (Figure 1), anammox would account for approximately 30% of N_2 production in the ODZ solely based on reaction stoichiometry for canonical organic matter composition (Devol, 2003). However, variations in the organic matter composition (Babbin et al., 2014), differences in the oxygen inhibition of denitrification and anammox reactions (Dalsgaard et al., 2014), or existence of other metabolisms (Babbin, Buchwald, et al., 2020; Lam et al., 2009) could alter the proportion N_2 production attributable to anammox. Elucidating the denitrification-anammox dichotomy is critical for understanding the connection between the global nitrogen cycle and climate. Denitrification is a significant marine natural source of nitrous oxide (N_2O) (Babbin et al., 2015; Babbin, Boles, et al., 2020; Ji et al., 2015), which is a key greenhouse gas and stratospheric ozone-depleting substance in the atmosphere (Naqvi et al., 2000; Ravishankara et al., 2009). In addition, anammox and denitrification have a differential impact on dissolved inorganic carbon (DIC) chemistry because autotrophic processes such as anammox consume DIC, whereas heterotrophic processes such as denitrification release DIC. Denitrification can admittedly also occur as an autotrophic process involving the sulfur redox chemistry (Fuchsman et al., 2017; Raven et al., 2021; Saunders et al., 2019), or methane oxidation (Thamdrup et al., 2019). However, in ODZs autotrophic denitrification is less significant compared to heterotrophic denitrification, so it is neglected in this study. Furthermore, recent studies assessing anammox and denitrification rates with incubation experiments suggest that the organic matter (OM) supply and composition play a critical role in the relative contributions of anammox and denitrification to nitrogen loss (Babbin et al., 2014; Chang et al., 2014; Ganesh et al., 2015; Kalvelage et al., 2013; Ward, 2013).

Nitrite profiles in ODZs differ markedly from the oxygenated global ocean. In the ODZs, nitrite accumulates in the water column at two distinct horizons: (a) the primary nitrite maximum (PNM) at the base of the euphotic zone, which also occurs globally and (b) the secondary nitrite maximum in the anoxic core, which is restricted to ODZs (Brandhorst, 1959; Buchwald & Casciotti, 2013; Buchwald et al., 2015; Lipschultz et al., 1996). The formation of the PNM is typically related to light-limited phytoplankton assimilation of nitrate or an imbalance of aerobic ammonium and nitrite oxidation (Buchwald & Casciotti, 2013; Lomas & Lipschultz, 2006; Zakem et al., 2018) and is outside the scope of this article. Nitrite accumulation in the anoxic core results from the rate differences between nitrite sources, that is, dissimilatory nitrate reduction to nitrite (DNRN), and sinks, that is, nitrite reduction via denitrification or anammox and nitrite (re)oxidation. Both direct rate measurements of denitrification and natural abundance isotopic analyses report that rapid recycling of nitrate (NO_3^-) and nitrite by DNRN and nitrite oxidation is dominant compared to nitrite reduction at the top of the ODZ (Babbin et al., 2017; Buchwald et al., 2015; Füssel et al., 2012; Kalvelage et al., 2013; Peters et al., 2016). Since the discovery of nitrite oxidation in the ODZs (Füssel et al., 2012), multiple studies have attempted to provide a possible mechanism for nitrite oxidation in the anoxic core, such as intrusion of oxygenated water masses (Bristow et al., 2016; Tsementzi et al., 2016), oxygen production by *Prochlorococcus* (Garcia-Robledo et al., 2017), oxidation by iodate and metals (Babbin et al., 2017; Evans et al., 2020; Hardisty et al., 2021; Moriyasu et al., 2020), nitrite dismutation (Babbin, Buchwald, et al., 2020), and anaerobic nitrite oxidation by anammox bacteria (Brunner et al., 2013). Understanding the relative distribution of nitrite oxidation in the ODZ core can significantly improve the understanding of the source and mechanism of nitrite oxidation.

Marine ODZs also exhibit unique inorganic carbon chemistry compared to the oxygenated pelagic ocean, containing, for instance, some of the lowest pH waters in the open ocean and correspondingly shallowest aragonite and calcite saturation horizons (Hernandez-Ayon et al., 2019; Jiang et al., 2019; Millero, 2007). Due to the long residence time accumulating remineralization products, these waters contain very high dissolved inorganic carbon (DIC) resulting from aerobic respiration and correspondingly low pH. High DIC concentrations up to $2,350 \mu\text{mol kg}^{-1}$ and in situ pH (total scale) values below 7.5 at 50 m depth have previously been reported in the Eastern Tropical South Pacific ODZ (Hernandez-Ayon et al., 2019; Paulmier et al., 2011), and similar features such as approximately $2,300 \mu\text{mol kg}^{-1}$ DIC and pH below 7.6 are observed in historical data, such as the P18 WOCE section sampled during CLIVAR and GO-SHIP, from the ETNP (Lauvset et al., 2021; Olsen et al., 2020). Calcite and aragonite are calcium carbonate ($CaCO_3$) minerals produced by phytoplankton such as coccolithophores, zooplankton such as pteropods, and protozoans such as foraminifera. The dissolution of calcium carbonate has a buffering effect on ocean acidification, impacts the ocean's ability to absorb CO_2 from the atmosphere (Feely et al., 2002), and acts to ballast sinking organic material. Furthermore, in situ pH

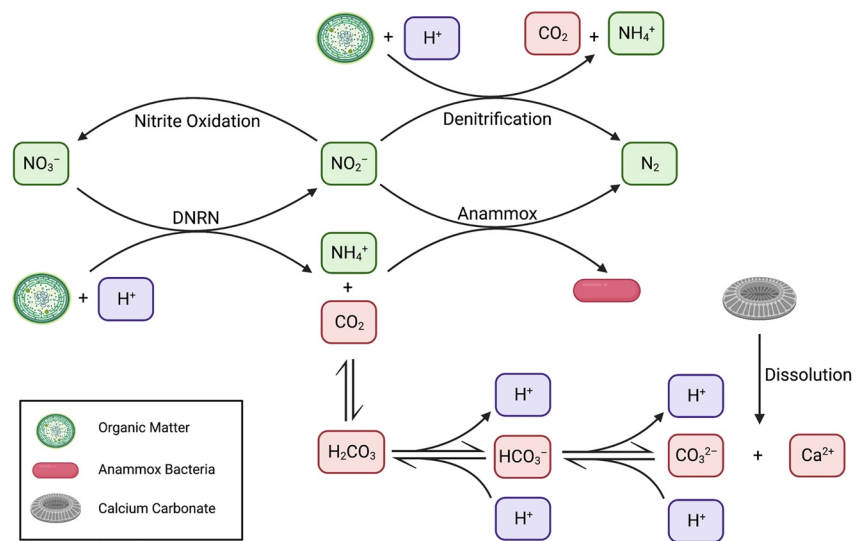


Figure 1. Conceptual illustration of the major nitrogen and carbon cycling reactions in the ETNP ODZ. Dissolved inorganic nitrogen species are colored green, dissolved inorganic carbon species are colored red, and protons are colored purple. Heterotrophic processes are represented as consuming organic matter and releasing CO_2 and NH_4^+ , while autotrophic processes are represented as consuming CO_2 and NH_4^+ and producing organic matter.

conditions are thought to affect the dissolution of biogenic CaCO_3 particles by impacting the DIC speciation and CO_3^{2-} concentrations in the water column (Millero, 2007). Classically, saturation state (Ω) has been defined to indicate a thermodynamic tendency for calcium carbonate to precipitate ($\Omega > 1$) or dissolve ($\Omega < 1$). However, the dissolution of CaCO_3 cannot be simplified to just ambient pH, and saturation conditions as prior studies suggest that mineral structure and other biogeochemical dynamics play significant roles in modifying dissolution kinetics and distribution (Adkins et al., 2021; Milliman et al., 1999; Pan et al., 2021; Subhas et al., 2022; Woosley et al., 2012). Consequential to low pH, aragonite saturation horizon depths (where $\Omega = 1$, see Equation 6) shallower than 100 m are notably observed in ODZs (Feely et al., 2002; Hernandez-Ayon et al., 2019).

Even though inorganic nitrogen and carbon chemistry in the ODZs are interconnected, there are few data from ODZs examining the interrelated cycling of these elements or investigating the impact of denitrification on pH in these waters. While denitrification of nitrite accompanied by the respiration of sinking organic matter in ODZs releases CO_2 , potentially decreasing pH, it also consumes protons and produces alkalinity (Koeve & Kähler, 2010), which can counterbalance the pH decrease. In addition, sulfate reduction (Jørgensen, 1982; Raven et al., 2021) and particle- or zooplankton-associated methanogenesis (Sasakawa et al., 2008; Schmale et al., 2018) can impact the biogeochemistry in the ODZ. However, the contributions from such processes are typically negligible in comparison to nitrogen metabolisms (Raven et al., 2021; Schmale et al., 2018) and excluded from this analysis of the major biogeochemical pathways. Understanding the interrelated cycling of DIN and DIC requires simultaneous and spatially high-resolution measurements that can reveal sharp chemical gradients in the ODZs. High-resolution measurements ensure that the critical features such as local extrema or large vertical changes in nutrient and pH profiles are accurately represented so that the critical link between DIN and DIC cycles can be resolved.

Here, we present a novel framework for studying ODZ biogeochemistry and the nitrogen cycle, focusing on nitrite accumulation and pH increase across the broad SNM by investigating the coupling between inorganic carbon chemistry and the nitrogen cycle based on in situ biogeochemical measurements. Although prior process-based studies focus intensively on the ODZ nitrogen cycle with DIN measurements and by determining reaction rates from incubation experiments, they generally overlook DIC measurements and the role of pH in ODZ biogeochemistry. Such studies require perturbation or stimulation of natural populations and potentially indicate current local conditions alone (Dalsgaard et al., 2012; Ward et al., 2009). On the other hand, simultaneous DIC and DIN geochemical measurements represent the integrated net changes in a water parcel moving along an isopycnal surface within the ODZ over time. Therefore, a new term, relative contribution, is introduced in this study to represent the net effect of cumulative biogeochemical metabolisms in the ETNP ODZ. Relative contribution

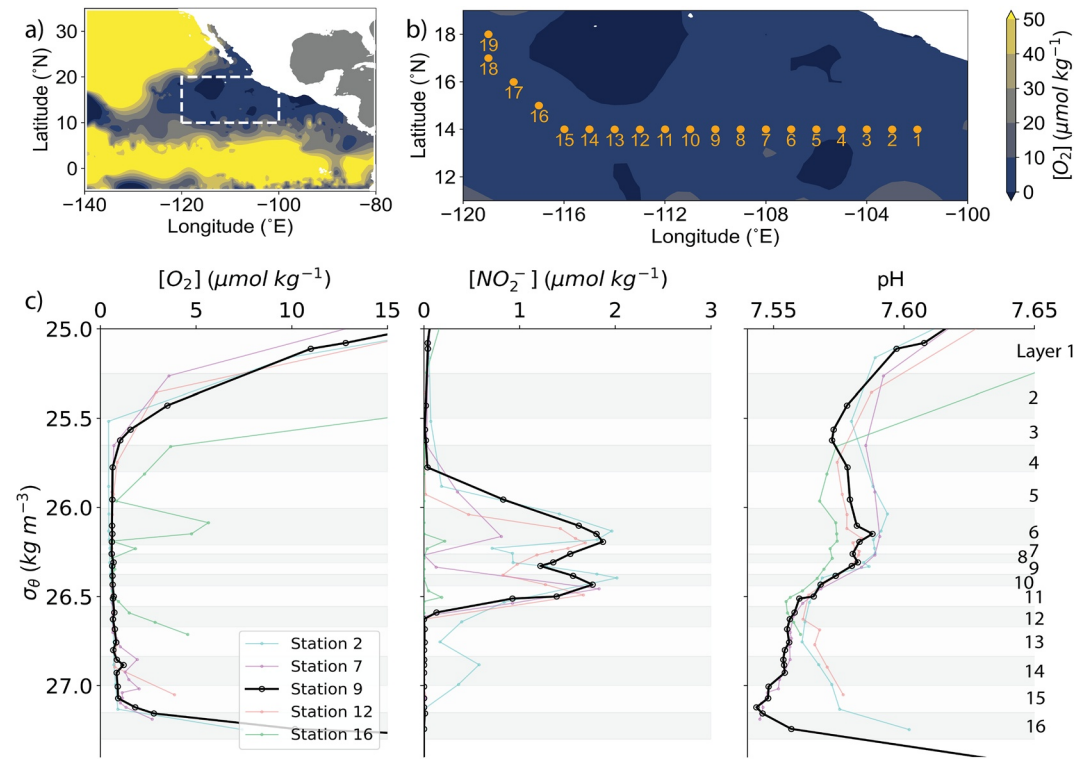


Figure 2. (a) Dissolved oxygen concentration at $\sigma_\theta = 26.2 \text{ kg m}^{-3}$ potential density surface in the Eastern Tropical North Pacific. Gridded O_2 concentration data are from Kwiecinski and Babbin (2021). The area enclosed by dashed lines is plotted separately in panel (b) with the *R/V Falkor* cruise track overlaid on the oxygen concentration contours. Interpreting the dissolved oxygen data is performed using the `inpaint_nans()` function on MATLAB R2021b (D’Errico, 2022). (c) Oxygen, nitrite, and pH vertical profiles in the ETNP ODZ ($25.0 < \sigma_\theta < 27.4 \text{ kg m}^{-3}$) for a representative collection of stations. Figure S2 in Supporting Information S1 shows the same profiles with depth (dbar) as the y-axis. The background shading indicates 16 layers, starting with layer 1 at the top, defined based on the three profiles. See Table S1 in Supporting Information S1 for potential density anomaly and depth ranges for each layer.

refers to the proportional effect metabolic reactions have in producing or consuming a shared reference tracer. For example, the relative contribution of anammox, compared to denitrification, is the proportion of fixed nitrogen lost via anammox relative to the total N_2 production by anammox and denitrification combined. We assess the relative contribution of key reactions, including DNRN, nitrite oxidation, nitrite reduction to N_2 via canonical heterotrophic denitrification (referred to as denitrification from this point onward), anammox, and calcium carbonate dissolution by constraining observed changes in DIN and DIC concentrations and speciation. Building on prior work, we investigate the correlation between the relative contribution and organic matter content by varying the carbon oxidation state and C:N:P ratio in a model framework based on literature values. Lastly, we compare observations to a hypothetical water pH profile to investigate the impact of denitrification on observed pH in the ETNP ODZ and CaCO_3 saturation state in the water column.

2. Methods

2.1. Sample Collection, Tracer Measurements, and Data Analysis

The present study focuses on data collected during a research cruise on *R/V Falkor* (FK180624) in the Eastern Tropical North Pacific (ETNP) in June–July 2018. Additionally, nitrite, pH, alkalinity, and oxygen data from the AT37-12 cruise on *R/V Atlantis* in the southern part of the ETNP in April–May 2017 are presented as Supporting Information S1 (Data Set S1). Samples at various depths were acquired using a 24-bottle CTD rosette equipped with temperature, salinity, pressure, and oxygen sensors at 19 stations while focusing on the upper 1 km during the FK180624 cruise (Figure 2). The same sample acquisition method was followed during AT37-12 for 8 stations (Figure S1 in Supporting Information S1). All stations mentioned in the main text and presented in

the main figures belong to FK180624. AT37-12 data (Data Set S1) are presented for comparison in Supporting Information S1.

Total alkalinity (TA) was collected in borosilicate glass bottles and poisoned immediately with 0.02% mercuric chloride. Samples were stored in the dark at room temperature and measured in the lab following the cruise using a custom-designed open-cell titration system designed and built by the laboratory of Andrew G. Dickson (Scripps Institution of Oceanography) following best practices (Dickson et al., 2007). The pH was collected and poisoned in the same manner as TA but measured onboard within 6 hr of collection. A custom-designed automated spectrophotometric system similar to Carter et al. (2013) using an Agilent 8454 UV-Vis spectrophotometer was used to measure the pH on the total scale at 25°C with purified meta-cresol purple indicator provided by Robert H. Byrne (University of South Florida). More details of the system can be found in Woosley (2021). Nitrite, ammonium, and phosphate measurements were made spectroscopically with a 10 cm quartz cell and Ocean Optics QE Pro spectrometer (Babbin et al., 2014; Strickland & Parsons, 1972). NO_x^- (total nitrite and nitrate) measurements were performed using a Teledyne T200 analyzer via the standard chemiluminescence protocol (Babbin & Ward, 2013; Braman & Hendrix, 1989).

Physical seawater properties such as potential temperature (θ), density (ρ), and potential density anomaly referenced to the surface (σ_θ) were calculated using the TEOS-10 GSW package (Firing et al., 2021). Dissolved inorganic carbon (DIC) and in situ pH calculations were done by PyCO₂SYS package version 1.8 for Python 3.8 (Humphreys et al., 2020; Van Heuven et al., 2011). Dissociation constants K_1 and K_2 were based on Lueker et al. (2000). The total boron constant of Lee et al. (2010) and the K_{HF} of Perez and Fraga (1987) were used.

2.2. Organic Matter Composition and Reaction Stoichiometry

The chemical composition of organic matter sinking to the ODZ during our occupation was estimated by calculating the relative changes in nutrient, DIC, and apparent oxygen utilization (AOU) along the oxycline surface across all 19 stations. Admittedly, relative changes in nutrients, DIC, and AOU are impacted by processes other than the organic matter remineralization such as vertical diffusion and lateral mixing. Therefore, determining the organic matter composition using relative changes in nutrients, DIC, and AOU in the oxycline surface is a simplification and estimate for this region at the time of sampling. Nevertheless, the sensitivity analyses in the later sections with standard organic matter formulations show similar results. The oxycline was defined between 45 and 95 dbar pressure based on the water column oxygen profile (Figure S4a in Supporting Information S1). The study focuses on stations 1–14, excluding station 5 for further analysis because (a) stations 5, 15, and 17 are impacted by mesoscale eddies that can alter the water column structure and chemistry (Figure S5 in Supporting Information S1) and (b) stations 16, 18, and 19 have the lateral intrusion of oxygenated water masses at the top of ODZ (Figure S3a in Supporting Information S1). These layers diverge from the canonical definition of the ODZ due to oxygen intrusion and have a different water column chemistry. DIC, DIN, and oxygen concentration data from the selected stations were fitted against phosphate concentration in the oxycline using robust regression with Huber's t M-estimation method available on the Scikit-learn package (Pedregosa et al., 2011). Huber's t robust regression assigns varying weight values to outliers based on the predicted residual values, reduces the contribution of outliers to the regression, and increases the accuracy of slope value (Huber, 1973).

Sinking organic matter (OM) composition was calculated from the resulting C:N:P ratio following Moreno et al. (2020) and Paulmier et al. (2009). Stoichiometric coefficients for remineralization of the OM via DNRN and denitrification (Koeve & Kähler, 2010) and autotrophic anammox reaction (Strous et al., 1998) were determined from previous studies. Generic nitrite oxidation to nitrate without prescribing a specific oxidant and the calcium carbonate dissolution reaction were added to the list of key reactions occurring within the ODZ (Table 1).

The variables a – e in Table 1 refer to the elemental ratios of the organic matter remineralized in the ODZ. These variables are used to calculate stoichiometric coefficients of nitrate, nitrite (x and z), and water (y and w) in DNRN and denitrification reactions based on Koeve and Kähler (2010). Additionally, the $(b-2c)$ term refers to the hydrogen content of the organic matter with respect to the oxygen content. Since organic matter hydrogen and oxygen content cannot be assessed in our data, the $(b-2c)$ term was set by balancing the oxidation states for the organic matter. The C_{ox} term refers to the oxidation state of organic carbon and was calculated from the respiration quotient that describes the molar ratio of oxygen to organic carbon consumed during the aerobic respiration (Moreno et al., 2020). Oxygen consumption to phosphate production ratio ($r_{\text{AOU:P}}$) in the oxycline was used to

Table 1
Key Reactions Observed in the ETNP ODZ for the Generic Organic Matter (OM) Composition $C_a H_b O_c N_d P_e$

Process	Chemical reaction
DNRN	$OM + xNO_3^- + dH^+ \rightarrow aCO_2 + dNH_4^+ + eH_3PO_4 + xNO_2^- + yH_2O$
Denitrification	$OM + zNO_2^- + (z + d)H^+ \rightarrow aCO_2 + dNH_4^+ + eH_3PO_4 + \frac{z}{2}N_2 + wH_2O$
Anammox	$NH_4^+ + 1.32NO_2^- + 0.11CO_2 + 0.02H^+ \rightarrow N_2 + 0.11OM^{amx} + 1.90H_2O + 0.3NO_3^-$
Nitrite Oxidation	$NO_2^- + \text{Oxidant} \rightarrow NO_3^- + \text{Reductant}$
CaCO ₃ Dissolution	$CaCO_3 \rightarrow Ca^{2+} + CO_3^{2-}$

Note. $C_{ox} = 4 - \frac{4[(r_{AOU:P})^{-2d}]}{a}$, $(b - 2c) = (3d - aC_{ox} - 5e)$, $x = [2a + 0.5(b - 2c) - 1.5d + 2.5e]$, $y = [0.5b - 1.5d - 1.5e]$, $z = [\frac{4}{3}a + \frac{1}{3}(b - 2c) - d + \frac{5}{3}e]$, $w = [\frac{2}{3}a + \frac{2}{3}b - \frac{1}{3}c - 2d - \frac{2}{3}e]$.

calculate C_{ox} because the respiration quotient is restricted to the amount of oxygen consumed by aerobic respiration and nitrification in oxic environments.

2.3. Relative Reaction Rates and Relative Contribution Calculations

Based on the observed vertical oxygen, nitrite, and pH profiles, the suboxic ETNP water column ($25.0 < \sigma_\theta < 27.4 \text{ kg m}^{-3}$) was divided into 16 layers (isopycnal surfaces) to calculate the relative contribution of five key reactions (DNRN, nitrite oxidation, denitrification, anammox, and calcium carbonate dissolution) to the biogeochemical cycling of DIN and DIC in the ODZ (Table S1 in Supporting Information S1). It is important to note that the anoxic core of the ODZ is narrower than the full range of 16 layers, typically covering only layers 3–14 (Figure 2c and Figure S2 in Supporting Information S1). Initially, 8 layers were defined based on oxygen, nitrite, and pH data from stations 1–14, excluding station 5. Then, each layer was divided into two to capture the spatial resolution in the results while balancing the number of data points at each layer. For the 16 layers, the change in five tracer concentrations was calculated with respect to changes in DIC. The tracers were nitrate (NO_3^-), nitrite (NO_2^-), ammonium (NH_4^+), N^* , and total alkalinity (TA). The quasi-conservative N^* tracer refers to the relative DIN deficiency relative to phosphate based on the N:P ratio in the organic matter (Equation 1) (Deutsch et al., 2001; Gruber & Sarmiento, 1997).

$$N^* = ([NO_3^-] + [NO_2^-] + [NH_4^+]) - r_{N:P} [PO_4^{3-}] + 2.9 \mu\text{mol kg}^{-1} \quad (1)$$

The tracer concentrations within a layer were plotted against DIC using Huber's t M-estimation method (Pedregosa et al., 2011), which accounts for outliers in each isopycnal layer separately. The slope of the regression fit is denoted as Δtracer (formally, this is the change in the tracer quantity normalized per unit change of DIC). Assuming Δtracer values are impacted only by the five key reactions in the ODZ, Δtracer is a linear combination of each tracer's stoichiometric coefficients in each reaction (Equation 2). Subscripts i refer to tracers, including DIC, and j refer to five key reactions. R is a 6-by-5 matrix that combines each tracer's stoichiometric coefficients and relative reaction rates (referred to as χ in the following equations) varying by layer. All the terms in Equation 2, including the relative reaction rates in χ matrix, are unitless because no time proxy was measured in the study. An example calculation is provided in Supporting Information S1. Reaction coefficients were calculated by solving the linear system of equations using a nonnegative least squares method (`scipy.optimize.nnls()` function) available on Python SciPy package (Virtanen et al., 2020).

$$\Delta\text{Tracer}_i = \sum_j (R_{i,j} \times \chi_j) \quad (2)$$

Building upon the relative reaction rates, the relative contribution (RC) of each reaction in a particular layer is calculated with respect to a reference tracer. For example, the relative contribution of denitrification and anammox reactions is calculated with respect to ΔNO_2^- (Equations 3 and 4). Expressions for the other relative contribution calculations are given in Supporting Information S1 (Equations S1–S10 in Supporting Information S1).

$$RC_{\text{denitrification}} = \frac{R_{NO_2, \text{denitrification}} \times \chi_{\text{denitrification}}}{R_{NO_2, \text{denitrification}} \times \chi_{\text{denitrification}} + R_{NO_2, \text{anammox}} \times \chi_{\text{anammox}}} \quad (3)$$

$$RC_{\text{anammox}} = 1 - RC_{\text{denitrification}} \quad (4)$$

The error in the relative reaction rates (χ) and RC values was assessed by Monte Carlo simulations ($n = 10,000$), as follows. A Δ tracer value was randomly selected from the normal distribution defined based on the robust fit regression results, then used to calculate relative reaction rates and RC values as described above. χ and RC values are reported as the mean of 10,000 such simulations with one standard deviation (1 s.d.) of the simulation.

2.4. Expected Δ pH Calculation in the Presence of Denitrification

Based on Table 1 and Table S2 in Supporting Information S1, denitrification consumes protons, hence increasing pH. However, CO_2 released due to denitrification speciates in the water column, releasing protons and decreasing pH. Overall, net proton consumption and pH increase is expected based on the denitrification stoichiometric coefficients (Table 1 and Table S2 in Supporting Information S1). To estimate the net pH increase (Δ pH) at the top of the ODZ due to denitrification, in situ pH per organic carbon remineralized is calculated for an approximate range of total alkalinity (2,200–2,450 $\mu\text{mol kg}^{-1}$) and DIC (2,000–2,400 $\mu\text{mol kg}^{-1}$) observed in the ETNP based on GLODAP v2.2021 (Lauvset et al., 2021; Olsen et al., 2019, 2020). Some specific combinations plotted, for example, low DIC and high total alkalinity or high DIC and low total alkalinity are unlikely to be observed. Δ pH represents the increase in pH due to denitrification compared to a baseline case assuming no water-column denitrification. In situ pH values are determined using the PyCO₂SYS package with set temperature (11°C), salinity (35), and pressure (300 dbar) inputs selected as representative values in the ETNP ODZ.

2.5. Water Column pH and CaCO₃ Saturation State

Observed in situ pH data from the selected stations are fitted as a function of depth (z) between 50 and 900 dbar with a linear combination of exponential decay and Gaussian curve using ordinary least squares (scipy.optimize.curve_fit() function) available on SciPy package (Equation 5) (Virtanen et al., 2020). Exponential decay is parameterized by an amplitude (a) and a decay coefficient (b). The Gaussian function is parameterized by the amplitude (c), mean (d), and spread (e) variables. Since pH values converge to a constant value rather than zero at depth, an additional constant (f) is also included. Then, a hypothetical pH curve is constructed with an exponential decay function that approximates a hypothetical pH profile with no local pH maximum arising from denitrification (i.e., pH reflects only oxygen concentrations).

$$\text{pH} = ae^{-bz} + ce^{-\frac{(z-d)^2}{2e^2}} + f \quad (5)$$

For both pH curves, calcite and aragonite saturation state (Ω) (Equation 6) were derived using PyCO₂SYS (Humphreys et al., 2020) for in situ temperature, salinity, and pressure conditions in the ETNP ODZ.

$$\Omega = \frac{[\text{Ca}^{2+}][\text{CO}_3^{2-}]}{K_{sp}^{\text{CaCO}_3}} \quad (6)$$

3. Results

3.1. Oxygen, Dissolved Inorganic Nitrogen, Alkalinity, and pH Profiles in the ETNP ODZ

Oxygen concentration data for the collection of stations suggest that the anoxic ODZ in the ETNP is located approximately between $\sigma_\theta = 25.50$ and 26.67 kg m^{-3} potential density surfaces (Figure 2c). An intrusion of oxygenated water masses is also observable for stations 16 and 19. Based on the nitrite profiles for each station (Figure 3a) and the profile for the collection of stations, nitrite starts accumulating at layer 5 and peaks at $\sigma_\theta = 26.15 \pm 0.06 \text{ kg m}^{-3}$ (1 s.d.) initially and at $\sigma_\theta = 26.43 \pm 0.06 \text{ kg m}^{-3}$ (1 s.d.) for a second time before nitrite is consumed as oxygen concentration starts increasing again. Due to the existence of a local nitrite minimum (LNM) in concentration at $\sigma_\theta = 26.27 \pm 0.10 \text{ kg m}^{-3}$ (1 s.d.), we define the upper peak as SNM and the lower peak as a tertiary nitrite maximum (TNM), although note that canonically the secondary nitrite maximum refers to the full swath of nitrite accumulation rather than an individual specific maximum. Furthermore, pH increases at the top of the ODZ (layers 3–6), coincident with the accumulation of nitrite, to a peak that coincides with the SNM (Figures 2c and 3b) except for stations where oxygen intrusions are observed (Figure S3 in Supporting

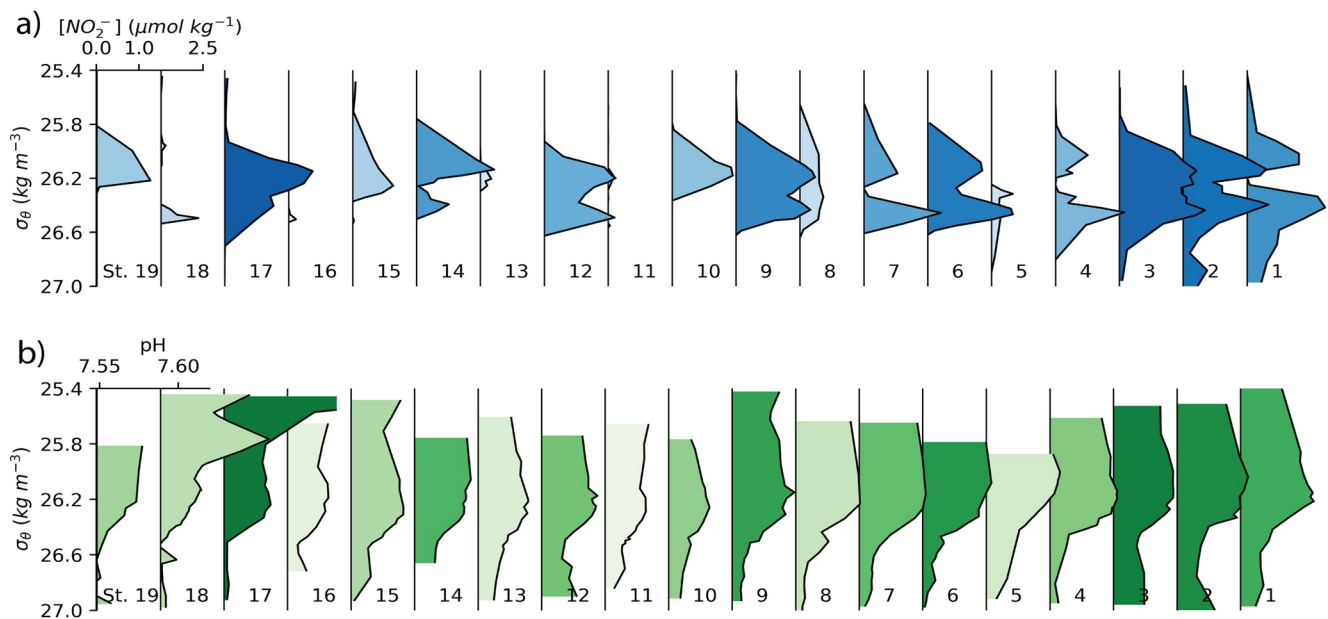


Figure 3. (a) Vertical nitrite and (b) pH profiles between $\sigma_{\theta} = 25.4$ and 27.0 kg m^{-3} at each station, respectively. Color for each station is based on the maximum nitrite concentration and pH values within the σ_{θ} range. Darker colors denote higher nitrite concentrations and pH values.

Information S1). In a smaller subset of stations, such as station 9, an additional increase in pH is observed below the local pH maximum, coinciding with the LNM.

Furthermore, similar two-peaked nitrite profiles can be observed in the anoxic core of a previous ETNP occupation in 2017 (Figure S1 in Supporting Information S1). However, prominent oxygen intrusions observed around 200 m in the southernmost stations reduce the thickness of the anoxic core. A narrower ODZ and prominent oxygen intrusions have been previously reported in the southern ETNP (Kwiecinski & Babbitt, 2021; Margolskee et al., 2019) and are responsible for differences in nitrite accumulation among different stations in that previous occupation. Notably, however, the local nitrite minimum with concentrations below detection in station 1 from the AT37-12 cruise is observed at the same depths of a small ($<5 \mu\text{mol kg}^{-1}$) oxygen intrusion.

Station 9 (14°N , 110°W) was selected as the representative station for the ETNP ODZ because coincident nitrite and pH peaks are apparent in the upper ODZ core (Figure 4), and it can be compared to previously reported data along the P18 line at 110°W . Furthermore, increases in nitrate, phosphate, and alkalinity with increasing density were observed at this station, likely due to organic matter remineralization and calcium carbonate dissolution. In addition, ammonium is depleted (maximum of $0.03 \mu\text{mol kg}^{-1}$) in the ODZ, likely via autotrophic processes such as anammox, in agreement with previous studies (Widner et al., 2018). When compared to previous measurements (CLIVAR in 2007 and GO-SHIP in 2016) at the same location (Figure 5), similar ranges of oxygen, nitrite, and pH are recorded. However, sparse sampling previously did not permit distinct SNM and TNM of similar magnitudes to be observed in these studies, even though the density surface of the TNM aligns in all three cruises (Figure 5). Yet, the pH increase in the upper ODZ is apparent in both our and CLIVAR data. Local pH minima and maxima from both cruises are observed at the same density surfaces.

3.2. Organic Matter Composition and Key Reactions

Based on nutrient, oxygen, and DIC calculations in the oxycline, the C:N:P ratio was determined for this limited region at the time of sampling as 112.50 ± 4.25 : 11.40 ± 0.34 : 1 mol/mol (1 s.d). In addition, apparent oxygen utilization (AOU) normalized to phosphate OM content ($r_{\text{AOU:P}}$) was calculated as $107.47 \pm 0.97 \text{ mol/mol}$ (1 s.d.). If we assume that all the ammonium released during the respiration of organic matter is converted into nitrate via nitrification, the carbon oxidation state (C_{ox}) associated with the organic matter is $+0.99$ for the calculated $r_{\text{AOU:P}}$. On the other hand, if no nitrification is performed in the oxycline and AOU only represents the respiration, C_{ox} becomes $+0.18$. Since the rates of nitrification or anammox are unknown, both end-members for C_{ox} are

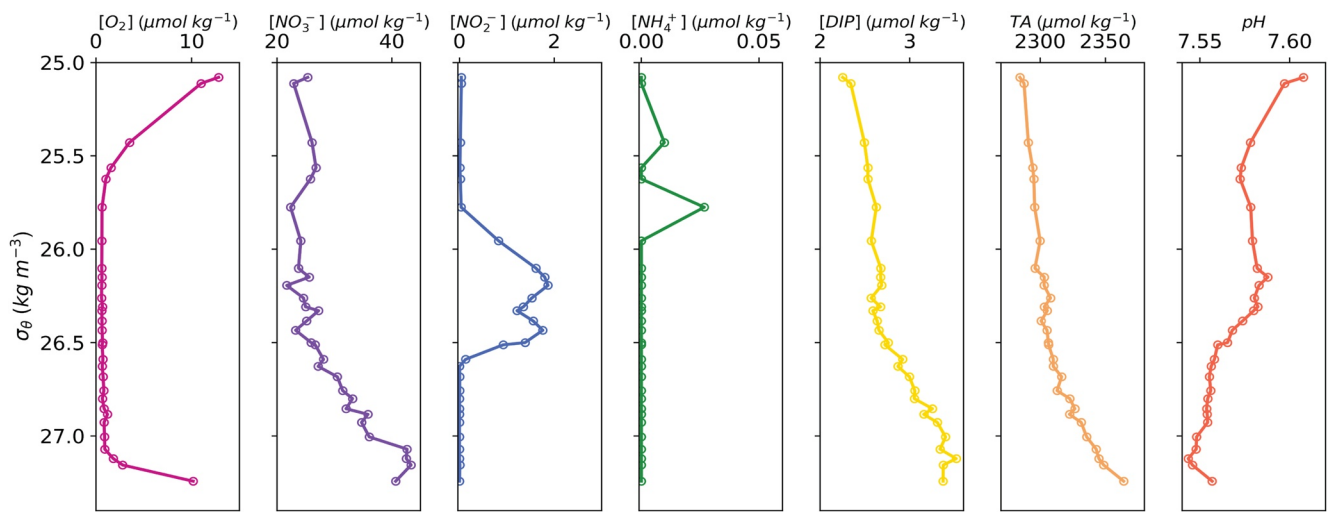


Figure 4. Measured tracer profiles at Station 9 during FK180624 research cruise. The accuracy of total alkalinity measurements was $0.11 \pm 1.77 \mu\text{mol kg}^{-1}$, determined from certified reference material (CRM). The TA precision was $\pm 2.28 \mu\text{mol kg}^{-1}$ determined from duplicates ($N = 46$). The precision of pH measurements was ± 0.0025 from ($N = 58$) duplicates. The precision of NO_x^- ($\text{NO}_2^- + \text{NO}_3^-$) was $\pm 0.035 \mu\text{mol kg}^{-1}$ from ($N = 39$) duplicates. The precision of nitrite (NO_2^-) measurements was $\pm 0.14 \mu\text{mol kg}^{-1}$ from ($N = 32$) duplicates. The precision of ammonium (NH_4^+) measurements was $\pm 0.056 \mu\text{mol kg}^{-1}$ from ($N = 32$) duplicates. The precision of dissolved inorganic phosphorus measurements was $\pm 0.46 \mu\text{mol kg}^{-1}$ from ($N = 32$) duplicates. Precision calculations with duplicates is based on Dickson et al. (2007).

examined. The results presented in the following sections correspond to C_{ox} of +0.99, and the results for C_{ox} of +0.18 are given in Supporting Information S1. Even though the analysis does not provide the exact oxygen and hydrogen content of the organic matter in both cases, the relative number difference of oxygen-to-hydrogen in the OM can be used to determine stoichiometric coefficients in DNRN and denitrification reactions (Table 1 and Table S2 in Supporting Information S1). The amount of water produced is not reported for balanced DNRN and

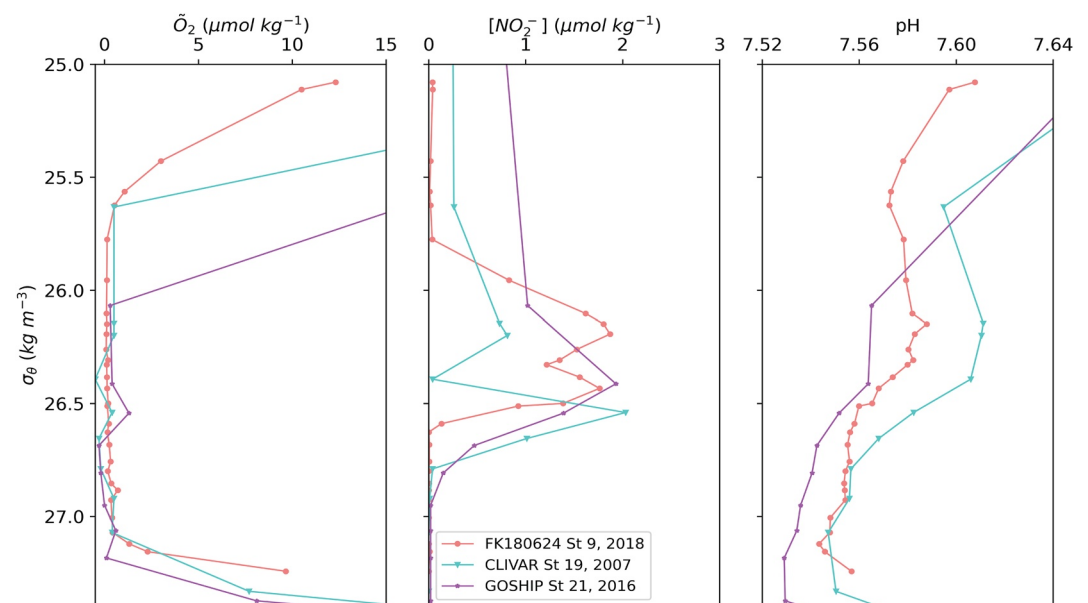


Figure 5. Vertical oxygen, nitrite, and pH profiles with respect to potential density anomaly in the Eastern Tropical North Pacific along the P18 line over a decade. CLIVAR and GO-SHIP P18 data are obtained from GLODAP v2.2021 (Lauvset et al., 2021; Olsen et al., 2019, 2020). GO-SHIP and CLIVAR P18 data are from cruises 33RO20161119 and 33RO20071215, respectively. Oxygen concentration data are shifted to align all the profiles at $0 \mu\text{mol kg}^{-1}$ in the ODZ core. Therefore, a new parameter $\tilde{\text{O}}_2$ is defined. 0.5, 3.2, and $2.5 \mu\text{mol kg}^{-1}$ is subtracted for each data point in FK180624, CLIVAR, and GO-SHIP, respectively, to $\tilde{\text{O}}_2$ parameter.

Table 2
Reaction Matrix (R) for the Sinking Organic Matter
($C_{112.5}H_bO_cN_{11.4}P_a$, $b - 2c = -82.17$, $C_{ox} = +0.99$)

Tracer	DNRN	Denitrification	Anammox	Nitrite oxidation	CaCO ₃ dissolution
ΔNO_3^-	-1.505	0.000	2.909	46.296	0.000
ΔNO_2^-	+1.505	-1.003	-12.000	-46.296	0.000
ΔNH_4^+	0.101	0.101	-9.091	0.000	0.000
ΔN^*	0.000	-1.003	-18.182	0.000	0.000
ΔTA	0.092	1.096	0.181	0.000	2.000
ΔDIC	1.000	1.000	-1.000	-1.000	1.000

Note. All the values are normalized to ΔDIC for each reaction.

nitrite denitrification reactions, but the biological production of H_2O has a negligible effect on the seawater chemistry. Based on the balanced reactions given the sinking organic matter composition, the reaction matrix (R), which represents the net change in a tracer due to reaction, is developed and shown in Table 2.

Since the specific nitrite oxidation mechanism is not yet resolved under anoxic conditions and is likely a combination of numerous pathways, a general reaction expression is used. A recent study of two marine nitrite-oxidizing bacteria (*Nitrospira moscoviensis* and *Nitrospina gracilis*) reports that 0.0216 mol of carbon are fixed via the reductive tricarboxylic acid (rTCA) cycle per mole of nitrite oxidized (Zhang et al., 2020). Therefore, a $\Delta DIC:\Delta NO_3^-$ of $-1:46.296$ is selected for the nitrite oxidation column in the R matrix. With the R matrix given in Table 2, relative reaction rates are calculated by nonnegative least squares solution for each layer (Figure S6 in Supporting Information S1).

3.3. Relative Contributions of Biogeochemical Reactions

Using set reaction stoichiometries and the observed changes in our inorganic nutrient tracers with respect to inorganic carbon, we calculate the reaction relative contribution (RC) to describe the distributions of key reactions in the ODZ and their proportional effect on the budget of a tracer (Figure 6). In terms of the loss of bioavailable fixed nitrogen (i.e., N_2 production), anammox accounts for between 34.9% and 79.2%, depending on the specific ODZ layer. Higher values are observed at the SNM and at the bottom of the ODZ. In the layers above and below the anoxic ODZ core, where oxygen is more abundant, anammox accounts for 98.5% of N_2 production compared

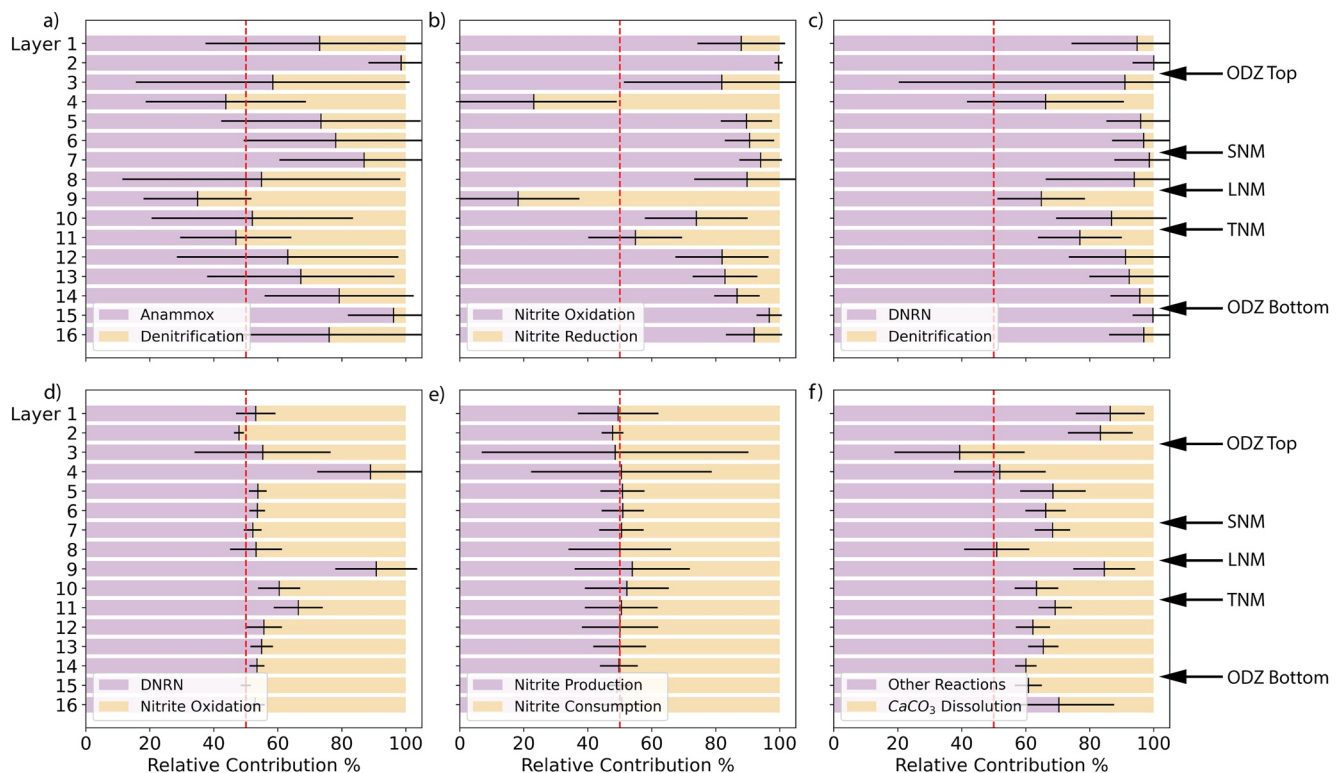


Figure 6. Relative contribution of key reactions to nitrogen and carbon chemistry in each of 16 layers in the ODZ. The results are for the organic matter with +0.99 carbon oxidation state. Secondary nitrite maximum (SNM), tertiary nitrite maximum (TNM), and local nitrite minimum (LNM), and ODZ boundaries are indicated with arrows on the right side. 50% value is marked with a vertical red dashed line. Reference tracer for panels a, b, c, e is nitrite. Reference tracer for panel d is nitrate. Reference tracer for panel f is dissolved inorganic carbon. Equations for calculating each relative contribution value are given in Equations 3 and 4 and Equations S1–S10 in Supporting Information S1.

with denitrification. Notably, the distribution of the denitrification and anammox reactions calculated here does not precisely agree with the findings from microbial studies in the region (Fuchsman et al., 2017), which suggest dominant denitrification over anammox at the top of the ODZ. The discrepancy can be attributed to the presence of denitrifying organisms on particles and differential activity by individual organisms. This distribution does agree well, however, with data from the direct incubations (Babbin, Buchwald, et al., 2020). From our calculations, the relative denitrification contribution peaks just below the local nitrite minimum (LNM, layer 9) with an RC of 65.1% compared to anammox. Yet, anammox and denitrification combining to reduce nitrite to dinitrogen are not generally the major consumption pathway for nitrite.

Nitrite oxidation typically accounts for over 80% of all nitrite consumption except just below the top of the ODZ and the LNM (layers 4 and 9). Yet, nitrite production via DNRN and its combined consumption from anammox, denitrification, and nitrite oxidation are typically close to balanced, with the slight net rate leading to the shape of the profiles observed. Indeed, the first step of canonical denitrification, DNRN, is always greater than denitrification from nitrite, supporting the concept of rapid recycling of nitrate in the ODZ. Comparing the rates of DNRN with nitrite oxidation directly, we find that nitrate reduction is between 1 and 10 times as large as nitrite oxidation, with peak DNRN to nitrite oxidation ratios at the top of the ODZ and just below the LNM, that is, both depth zones where nitrite accumulates. Finally, in comparing the production of DIC between net biological remineralization and calcium carbonate dissolution (Figure 6f), the contribution of CaCO_3 dissolution decreases with depth between the top of the ODZ and the LNM and increases below the LNM. CaCO_3 dissolution accounts for 15.5%–60.7% (but typically less than half) of DIC production in the ODZ, with a minimum in layer 9, which is found to be a hotspot of denitrification.

3.4. Variations in the Organic Matter Carbon Oxidation State and C:N:P Ratio

Since this study does not determine the amount of nitrification occurring in the oxycline, total oxygen consumption during the aerobic remineralization of organic matter is only partially constrained. Therefore, any organic matter C_{ox} value between the two end-members (+0.18 when no nitrification occurs and +0.99 when all the ammonium from respiration is oxidized to nitrate) is possible within the study domain based on AOU observations. However, the proposed C_{ox} values are outside the C_{ox} range observed across the Eastern Pacific determined by Moreno et al. (2020). Moreno et al. (2020) reports that the mean C_{ox} value in the ETNP along the P18 line (between ~ 10 and 20°N) is -0.76 , although their full range spans -1.92 to -0.32 in the ETNP. Since a wide range of oxidation states is reported, it is necessary to determine the effect of carbon oxidation state on the relative contribution. We repeated the relative contribution calculations in all 16 layers in the ETNP ODZ for C_{ox} values ranging between -2.5 and $+1.5$ with 0.5 increments. The wider C_{ox} range was selected based on C_{ox} observed globally in Moreno et al. (2020). In addition, we investigated the impact of C:N:P ratio on the relative contribution of all the key reactions in the ODZ by repeating each calculation for the Redfield C:N:P ratio (106:16:1) (Redfield, 1958) (Figure 7). The general vertical pattern that suggests higher nitrite reduction at the top of the ODZ and the LNM did not change when different C_{ox} and C:N:P ratios were used in the calculations (Section 3.3, Figures S7–S9 in Supporting Information S1). However, the specific balance of anammox, denitrification, and nitrite oxidation changed slightly for each layer, as shown in Supporting Information S1 and illustrated as the range of values for anammox %, nitrite oxidation to reduction ratio, and nitrite oxidation to DNRN ratio (Figure 7).

Anammox % (percentage loss of fixed nitrogen attributed to anammox), nitrite oxidation to reduction ratio, and nitrite oxidation to DNRN ratio are three critical values that show the impact of varying organic matter content on the relative contribution distribution by layer (Figure 7). Anammox % is mostly constant at different C_{ox} values except for at the top of the ODZ where the highest nitrite reduction contributions are observed. Therefore, we show that anammox % is strongly dependent on C_{ox} only at the top of the ODZ when C_{ox} is higher than zero. Anammox % for Redfield C:N:P ratio shows approximately a 10%–17% increase compared to that for OM with observed C:N:P ratio (112.5:11.4:1 mol/mol) in all the layers due to an increase in organic nitrogen content. Moreover, the ratio of nitrite oxidation to reduction for the generic organic matter decreases with increasing C_{ox} , and the change is more gradual at the top of ODZ compared to the other layers. Similarly, nitrite oxidation to DNRN ratio decreases with increasing C_{ox} , but more gradually for lower oxidation states. On the other hand, changing the C:N:P ratio does not vary the nitrite oxidation to reduction ratio and nitrite oxidation to DNRN ratio as much as anammox %.

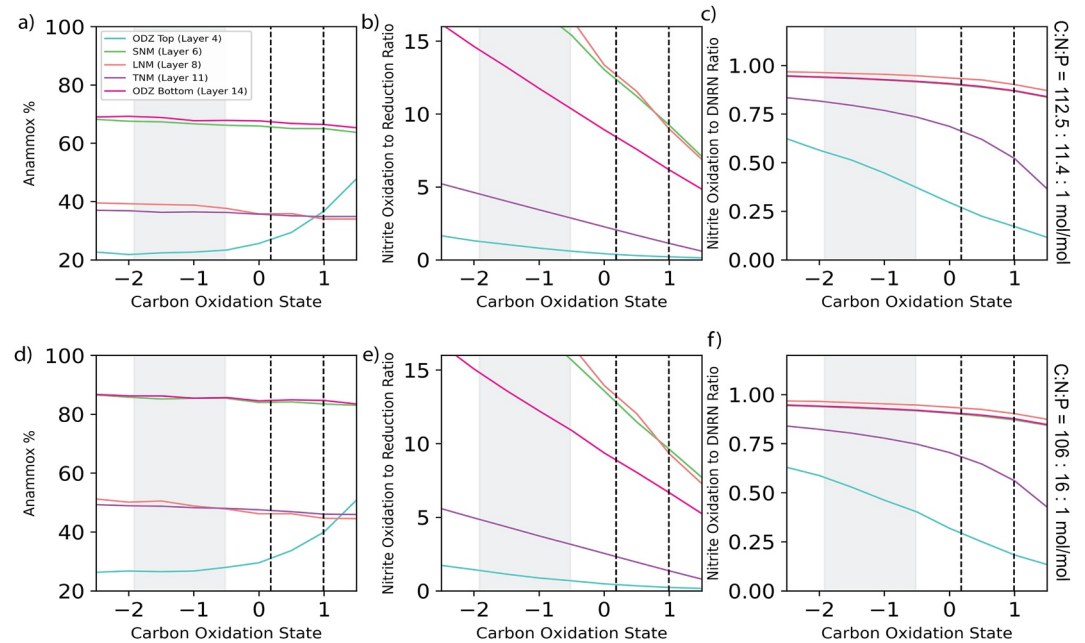


Figure 7. (a and d) Anammox % for nitrite reduction to N₂ compared to denitrification, (b,e) nitrite oxidation to nitrite reduction ratio, and (c,f) nitrite oxidation to DNRN ratio for four layers in the ETNP ODZ based on relative contribution analysis. Panels (a–c) are based on C:N:P ratio (112.5:11.4:1 mol/mol) calculated in this study and panels (d–f) are based on Redfield C:N:P ratio (106:16:1 mol/mol). Layers 4, 6, 7, 11, and 14 correspond to the top of the ODZ, secondary nitrite maximum, local nitrite minimum, tertiary nitrite maximum, and bottom of the ODZ, respectively. Gray shading represents the range of carbon oxidation states ($-1.92 < C_{ox} < -0.32$) reported by Moreno et al. (2020) in the ETNP and the dashed lines represent +0.18 and +0.99.

Moreover, C_{ox} affects the pH increase relative to a baseline case with no denitrification at the top of the ODZ through changes in denitrification RC% (Figure 8). For OM with +0.99 carbon oxidation state, the increase in pH due to denitrification is calculated by taking proton consumption and DIC release into account (Table S2 in Supporting Information S1) at various alkalinity and DIC conditions in the water column (Figure 8a). Even though CO₂ is produced by the denitrification reaction, simultaneous consumption of protons balances the pH decrease due to DIC production. As a result, a net increase in pH is observed for the OM with +0.99 carbon

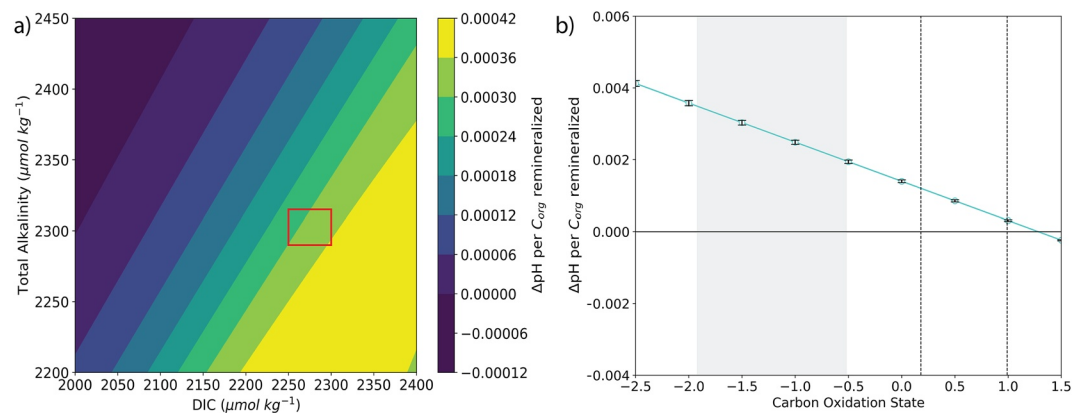


Figure 8. (a) Expected change in pH per organic carbon (C_{ox} = +0.99) remineralized at the top of ETNP ODZ due to denitrification compared to a baseline case with no denitrification for a range of TA and dissolved inorganic carbon (DIC) values. (b) Expected change in pH per organic carbon with varying oxidation state due to denitrification. Each data point represents the mean ΔpH within the red box on panel (a) which corresponds to observed TA and DIC values in the ODZ. Gray shading represents the range of carbon oxidation states ($-1.92 < C_{ox} < -0.32$) reported by Moreno et al. (2020) in the ETNP and the dashed lines represent +0.18 and +0.99.

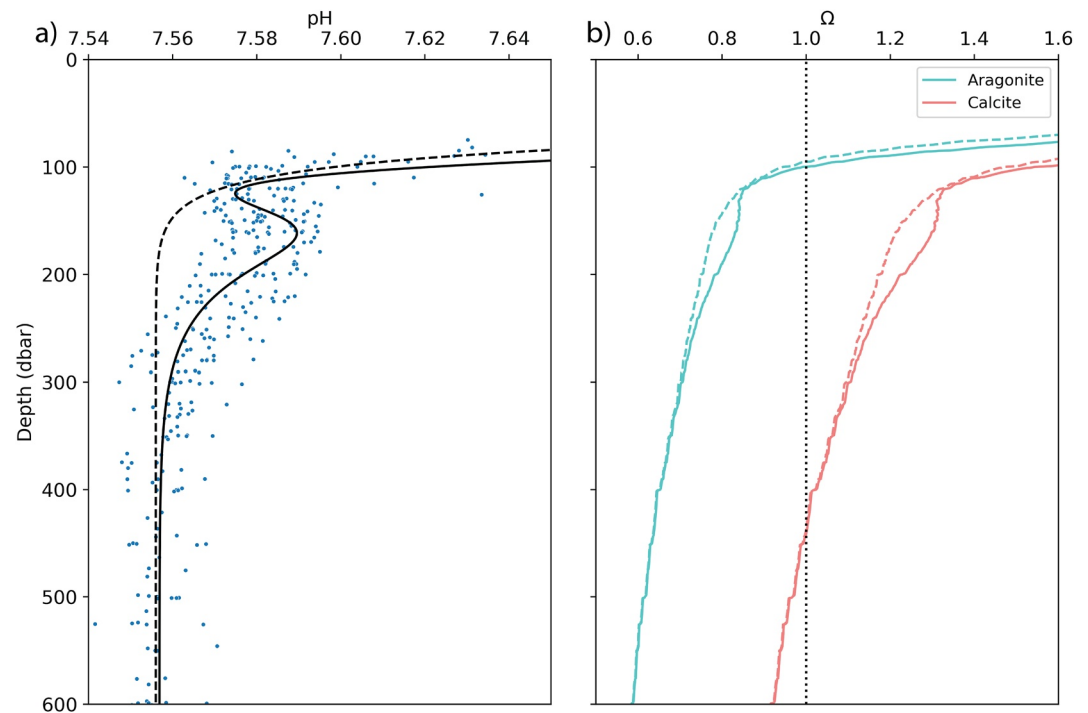


Figure 9. (a) pH and (b) aragonite and calcite saturation state depth profiles in the ETNP. Data collected in the study for the selected stations are represented as blue dots. Solid lines represent the fit to the data points while the dashed lines represent hypothetical scenario where no pH increase is observed at the top of the ODZ and there is no physical water mass mixing at depth.

oxidation state. For varying C_{ox} values, pH increase due to organic matter denitrification is observed below +1.27. On the other hand, other reactions, such as DNRN, consume fewer protons compared to those released via DIC production and result in a net pH decrease. Therefore, we can safely state that pH increase at the top of the ODZ signals nitrogen loss via denitrification of organic matter compositions reported in the ETNP ODZ because other key nitrogen cycle reactions cannot increase the pH.

3.5. pH and $CaCO_3$ Saturation State

Observed pH values are fitted with a function of depth as described in the methods. In addition, a theoretical exponential decay curve with depth is generated to represent a pH profile that closely tracks dissolved oxygen as elsewhere in the global ocean and where the observed increase at the top of the ODZ is absent. Using Equation 6, calcium carbonate saturation (Ω) is determined for each pH profile. In both cases, the aragonite saturation horizon ($\Omega = 1$) is found above the ODZ, whereas the calcite saturation horizon is found below the ODZ (Figure 9). In addition, differences in Ω between the baseline case with no denitrification and the one where denitrification is permitted are greatest at the local pH maximum as expected, showing that denitrification adds buffering capacity in the ocean. The Ω difference between two cases is notably larger for calcite compared to aragonite.

4. Discussion

4.1. High Resolution Nitrite and pH Measurements

Simultaneous measurements of inorganic nitrogen and carbon offer an integrative approach for resolving which metabolisms shape biogeochemistry in the ETNP ODZ. Our relative contributions terms represent the integrated impact of a reaction, as a water parcel traverses the ODZ instead of an instantaneous reaction rate at a specific location or time that can carry methodological artifacts due to the perturbation of natural microbial communities in incubation experiments. Changes in the total alkalinity, pH, and DIC complement DIN measurements in

Δ tracer calculations and allow further distinction between key reactions. As a result, the system of equations connecting DIN and DIC measurements with relative reaction rates (Equation 2) can be solved successfully.

Moreover, investigating ODZ biogeochemistry requires measurements with the high spatial resolution because the ODZ is not a single well-mixed box and consists of distinct biogeochemical regimes along different layers or isopycnal surfaces. For example, low-resolution CLIVAR and GO-SHIP measurements (Figure 5) either blend the SNM and TNM together or underrepresent the nitrite accumulation across the SNM, whereas high-resolution FK180624 data show two distinct coherent nitrite peaks. Due to the global nature of CLIVAR and GO-SHIP programs, only very low resolution of DIC and DIN measurements within the ODZs is typically permitted. These programs include only a few ODZ stations spanning the entire water column instead of focusing on the suboxic depths. Furthermore, the organic matter composition and size, which is a key factor impacting local relative contributions, vary significantly across the ETNP and with depth (Cram et al., 2022), and could alter the observed individual tracer profiles. Therefore, integrative approaches coupled with high-resolution data such as reaction relative contributions and high-resolution DIC and DIN measurements create a new standard for future investigations of ODZ biogeochemistry.

4.2. Nitrite Cycle in the ETNP ODZ

Using simultaneous DIN and DIC measurements, our study determined the composition of the organic matter sinking to the ODZ from the surface. The N:P ratio estimated for the organic matter sinking in the ETNP (11.4:1) is less than the canonical Redfield ratio (16:1) (Anderson, 1995; Redfield, 1958). The N:P ratio observed in the oxycline in the ETNP is considerably less than the Redfield N:P ratio because the fixed nitrogen in the water masses transiting the ODZ is consumed relative to phosphate via denitrification and anammox. These water masses upwell in the coastal areas of the ODZ to supply the surface ocean with similarly depleted fixed nitrogen and a low N:P ratio. We continue to find that anammox is the dominant pathway for nitrogen loss in the ETNP overall regardless of C_{ox} and C:N:P ratio, but the specific magnitude of anammox % depends on C:N:P ratio. Because denitrification, not anammox, produces the climatically important gas N_2O , the dependence of the contribution of denitrification to fixed nitrogen loss on the N-content of organic matter affects N_2O production. This organic matter remineralized in the ODZ can be sourced, in addition to sinking surface material, from marine organisms such as zooplankton migrating into ODZ (Bianchi et al., 2014; Cram et al., 2022). The composition of the zooplankton-derived organic matter is reported to be enriched in nitrogen compared to the canonical stoichiometry (Pitt et al., 2009; Ventura, 2006). The resulting lower C:N ratio would yield an increased anammox %, as suggested by Figures 7a and 7d in order to consume additional ammonium produced by DNRN and denitrification. Reconciling the organic matter supply to ODZs remains a long-standing need.

Denitrification relative contribution values imply that denitrification is within one order of magnitude of anammox, similar to other studies in the Pacific ODZs (Babbin et al., 2017; Babbin, Buchwald, et al., 2020; Peng et al., 2015). Other studies report that anammox, while affected, is less inhibited by oxygen than denitrification (Dalsgaard et al., 2014), which explains higher anammox relative contribution values at the anoxic-oxic interface (top and bottom 3 layers) in Figure 6. Calculated anammox % strongly depends on C_{ox} at the top of the ODZ, implying that denitrification is enhanced by higher carbon oxidation states when the environment is fully anoxic. The standard deviation in the relative contributions (Figure 6) is generated by the error in Δ tracer best fits for each layer. These standard deviation values also suggest that the total reduction of nitrite is better constrained than the partitioning between anammox and denitrification, potentially explaining why there is less agreement between previous studies regarding anammox % in the ODZs. Additionally, denitrification in anaerobic particles outside and within the anoxic core (Bianchi et al., 2018; Fuchsman, Paul, et al., 2019) could alter the relative contributions. Here, denitrification in particles is not distinguished from the water column as we solely ascertain integrated metabolic impacts on the water. Additionally, denitrification outside of the 16 layers is not investigated as the simple system of reactions (Table 2) does not capture the biogeochemistry outside the anoxic core and suboxic boundaries.

Even though our work does not directly determine changes in nitrite oxidation rate magnitudes with depth, the shape of nitrite oxidation relative contribution with respect to nitrite reduction and DNRN is consistent with studies in the ETSP and ETNP ODZ cores in which nitrite oxidation is more important at the edges of the ODZ (Babbin, Buchwald, et al., 2020; Peng et al., 2015, 2016). Furthermore, nitrite oxidation to reduction ratios are expected between 0 and 6.5 and nitrite oxidation to DNRN ratios are between 0 and 0.8 in the ETSP ODZ from

integrated natural abundance isotope surveys (Casciotti et al., 2013). The ratios calculated by our novel relative reaction contribution method fall within these ranges at the top of the ODZ and the TNM. Furthermore, the highest denitrification rates are likely to be observed at the ODZ top compared to the rest of the ODZ core (Babbin, Buchwald, et al., 2020). The low nitrite oxidation to reduction ratio also suggests that the ODZ top is more significant for fixed nitrogen loss in the ODZ compared to other layers. Recent studies report that the largest N_2 concentrations are found deeper within the ODZ (Fuchsman et al., 2018). The difference could be attributed to physical aspects such as the residence time of water masses and their chemical constituents or to a greater role in migrating zooplankton (Fuchsman et al., 2018), but it requires further investigation. Enhanced denitrification at the top is responsible for low nitrite concentrations in layers 3–4 due to increased nitrite consumption in these layers. Layers at the bottom of the ODZ and in the LNM show amplified nitrite oxidation suggesting a different water column chemistry than that of the anoxic core.

Moreover, a comparison between different biogeochemical regimes within the ODZ core (Figure 6) suggests that the SNM and TNM are distinct due to mainly the difference in anammox %. While the SNM has a higher anammox % and nitrite oxidation to reduction ratio, the TNM has a lower anammox % and nitrite oxidation to reduction ratio. Higher nitrite oxidation at the SNM is likely the cause of a decrease in nitrite concentration below the SNM, similar to the ecosystem oscillation trend in the ODZ core investigated by Penn et al. (2019) (see their Figure 3a). Furthermore, Penn et al. (2019) reported that physical oxygen supply at low nitrite and ammonium concentrations could induce an increase in nitrite by reestablishing the competitive advantage of aerobic organisms. Even though no detectable oxygen in the anoxic core is observed in the selected FK180624 stations at the time of sampling, physical intrusion of oxygenated water masses is observed in similar regions of the ETNP such as station 1 from AT37-12 cruise (Figure S1c in Supporting Information S1) and as reported previously (Kwiecinski & Babbin, 2021; Margolskee et al., 2019). Therefore, intrusions of oxygen at nanomolar concentrations might be a likely cause for the nitrite increase above the TNM.

4.3. Denitrification, pH, and Calcium Carbonate Dissolution in the Water Column

As illustrated in Figures 2–4, the pH peak at the top of the ODZ is coincident with SNM for the majority of stations. According to balanced reactions in Table 1, denitrification and calcium carbonate dissolution increase pH while the other reactions decrease pH, when accounting for both proton consumption and DIC speciation due to CO_2 release. DNRN also consumes protons; however, speciation of the DIC produced more than compensates for this pH increase. Since pH is increasing with depth at the top of ODZ, where denitrification and carbonate saturation are higher, it is likely that this locally higher pH arises due to denitrification rather than calcium carbonate dissolution affecting local chemistry. Indeed, predictions based on the reaction stoichiometries are also verified by the ΔpH calculations performed for denitrification in the ODZ. In addition, Figure 8 implies that nitrogen loss due to denitrification is responsible for the pH increase at the top of the ODZ, even at varying possible carbon oxidation states.

Under the observed average temperature, salinity, alkalinity, and phosphate profiles in the ODZ, ambient Ω of aragonite reaches saturation above the ODZ top, while that of calcite reaches saturation below the ODZ. However, metabolic processes such as organic matter remineralization or DNRN above the ODZ and on particles are likely to decrease local pH, and lower Ω further. For instance, the impact of local metabolism on Ω is reported to shift the saturation horizon for calcite to shallower depths that coincide closely with the ambient aragonite saturation horizon (Subhas et al., 2022). Further work into sinking organic matter and calcium carbonate chemistry at highly localized microscales is necessary to elucidate whether the denitrification-driven pH increase helps to preserve $CaCO_3$ and impact biogeochemistry and export.

5. Conclusion

High-resolution sampling in the top 1 km of the ETNP ODZ and high-precision measurements of nutrients, total alkalinity, and pH allowed for an investigation of biogeochemical features unique to ODZs. To explain the coincident pH and secondary nitrite maxima as well as the two-peaked structure of nitrite profiles in the anoxic core, we divided the ODZ into 16 layers and determined the spatial distribution of various nitrogen-cycle reactions and calcium carbonate dissolution in each layer. The results suggest that the SNM and TNM are two distinct features derived from variations in the contributions of anammox vis-à-vis denitrification and the ratio of nitrite

oxidation to its reduction. Since these distinct features were clearly observed and subsequently analyzed due to high-resolution sampling, future studies investigating the nitrogen cycle in the ODZs need to increase sampling frequency to better understand DIN dynamics in these regions. In addition, the correspondence between the relative contribution of nitrite oxidation and oxygen profiles from AT37-12 imply that the intrusion of oxygenated water masses is a potential source of the LNM and subsequent TNM. However, this study did not examine the role of other potential oxidants such as iodate, iron, or manganese, the in situ oxygen production by cyanobacteria, or other particle-associated processes such as sulfate reduction or methanogenesis. Furthermore, the pH increase at the ODZ top is attributed to the denitrification reaction considering increased denitrification relative rates at the ODZ top and net consumption of protons by the reaction. The pH increase implies that the dissolution of sinking calcium carbonate particles could be partially abated in the ODZ.

Data Availability Statement

Bottle data from the FK180624 cruise are available through BCO-DMO (<https://www.bco-dmo.org/dataset/832389>), and CTD (Sea-bird SBE-911+) data are available through Rolling Deck to Repository (<https://doi.org/10.7284/129668>). CTD data from AT37-12 are available through BCO-DMO (<https://www.bco-dmo.org/dataset/739098>), and bottle data from AT37-12 are included as a supplement (Data Set S1). GO-SHIP and CLIVAR P18 data are available from the GLODAP v2.2021 (Lauvset et al., 2021; Olsen et al., 2019, 2020), cruise numbers 33RO20161119 and 33RO20071215, respectively. The scripts used in analyzing FK180624 data, developing models in the study, and plotting important figures are available at https://github.com/tcinay/bablab_FK180624.git.

References

- Adkins, J. F., Naviaux, J. D., Subhas, A. V., Dong, S., & Berelson, W. M. (2021). The dissolution rate of CaCO₃ in the ocean. *Annual Review of Marine Science*, 13(1), 57–80. <https://doi.org/10.1146/annurev-marine-041720-092514>
- Anderson, L. A. (1995). On the hydrogen and oxygen content of marine phytoplankton. *Deep Sea Research Part I: Oceanographic Research Papers*, 42(9), 1675–1680. [https://doi.org/10.1016/0967-0637\(95\)00072-E](https://doi.org/10.1016/0967-0637(95)00072-E)
- Babbin, A. R., Bianchi, D., Jayakumar, A., & Ward, B. B. (2015). Rapid nitrous oxide cycling in the suboxic ocean. *Science*, 348(6239), 1127–1129. <https://doi.org/10.1126/science.aaa8380>
- Babbin, A. R., Boles, E. L., Mühle, J., & Weiss, R. F. (2020). On the natural spatio-temporal heterogeneity of South Pacific nitrous oxide. *Nature Communications*, 11(1), 3672. <https://doi.org/10.1038/s41467-020-17509-6>
- Babbin, A. R., Buchwald, C., Morel, F. M. M., Wankel, S. D., & Ward, B. B. (2020). Nitrite oxidation exceeds reduction and fixed nitrogen loss in anoxic Pacific waters. *Marine Chemistry*, 224, 103814. <https://doi.org/10.1016/j.marchem.2020.103814>
- Babbin, A. R., Keil, R. G., Devol, A. H., & Ward, B. B. (2014). Organic matter stoichiometry, flux, and oxygen control nitrogen loss in the ocean. *Science*, 344(6182), 406–408. <https://doi.org/10.1126/science.1248364>
- Babbin, A. R., Peters, B. D., Mordy, C. W., Widner, B., Casciotti, K. L., & Ward, B. B. (2017). Multiple metabolisms constrain the anaerobic nitrite budget in the Eastern Tropical South Pacific. *Global Biogeochemical Cycles*, 31(2), 258–271. <https://doi.org/10.1002/2016GB005407>
- Babbin, A. R., & Ward, B. B. (2013). Controls on nitrogen loss processes in Chesapeake Bay sediments. *Environmental Science & Technology*, 47(9), 4189–4196. <https://doi.org/10.1021/es304842r>
- Bianchi, D., Babbin, A. R., & Galbraith, E. D. (2014). Enhancement of anammox by the excretion of diel vertical migrators. *Proceedings of the National Academy of Sciences*, 111(44), 15653–15658. <https://doi.org/10.1073/pnas.1410790111>
- Bianchi, D., Weber, T. S., Kiko, R., & Deusch, C. (2018). Global niche of marine anaerobic metabolisms expanded by particle microenvironments. *Nature Geoscience*, 11(4), 263–268. <https://doi.org/10.1038/s41561-018-0081-0>
- Braman, R. S., & Hendrix, S. A. (1989). Nanogram nitrite and nitrate determination in environmental and biological materials by vanadium(III) reduction with chemiluminescence detection. *Analytical Chemistry*, 61(24), 2715–2718. <https://doi.org/10.1021/ac00199a007>
- Brandes, J. A., & Devol, A. H. (2002). A global marine-fixed nitrogen isotopic budget: Implications for Holocene nitrogen cycling. *Global Biogeochemical Cycles*, 16(4), 67–1–67–14. <https://doi.org/10.1029/2001GB001856>
- Brandhorst, W. (1959). Nitrification and denitrification in the eastern tropical North Pacific. *ICES Journal of Marine Science*, 25(1), 3–20. <https://doi.org/10.1093/icesjms/25.1.3>
- Bristow, L. A., Dalsgaard, T., Tiano, L., Mills, D. B., Bertagnolli, A. D., Wright, J. J., et al. (2016). Ammonium and nitrite oxidation at nanomolar oxygen concentrations in oxygen minimum zone waters. *Proceedings of the National Academy of Sciences*, 113(38), 10601–10606. <https://doi.org/10.1073/pnas.1600359113>
- Brunner, B., Contreras, S., Lehmann, M. F., Matantseva, O., Rollog, M., Kalvelage, T., et al. (2013). Nitrogen isotope effects induced by anammox bacteria. *Proceedings of the National Academy of Sciences*, 110(47), 18994–18999. <https://doi.org/10.1073/pnas.1310488110>
- Buchwald, C., & Casciotti, K. L. (2013). Isotopic ratios of nitrite as tracers of the sources and age of oceanic nitrite. *Nature Geoscience*, 6(4), 308–313. <https://doi.org/10.1038/ngeo1745>
- Buchwald, C., Santoro, A. E., Stanley, R. H. R., & Casciotti, K. L. (2015). Nitrogen cycling in the secondary nitrite maximum of the eastern tropical North Pacific off Costa Rica. *Global Biogeochemical Cycles*, 29(12), 2061–2081. <https://doi.org/10.1002/2015GB005187>
- Carter, B. R., Radich, J. A., Doyle, H. L., & Dickson, A. G. (2013). An automated system for spectrophotometric seawater pH measurements. *Limnology and Oceanography: Methods*, 11(1), 16–27. <https://doi.org/10.4319/lom.2013.11.16>
- Casciotti, K. L., Buchwald, C., & McIlvin, M. (2013). Implications of nitrate and nitrite isotopic measurements for the mechanisms of nitrogen cycling in the Peru oxygen deficient zone. *Deep Sea Research Part I: Oceanographic Research Papers*, 80, 78–93. <https://doi.org/10.1016/j.dsr.2013.05.017>

Acknowledgments

We are indebted to the captain and crew of the *R/V Falkor* and *R/V Atlantis* for their assistance at sea. We also thank the chief scientist Stefan Sievert on the AT37-12 cruise for enabling CTD sampling. We acknowledge the decades of scientists, marine technicians, ships' crew, and engineers who contributed to CLIVAR and GO-SHIP P18 cruises, and NOAA CoastWatch and OceanWatch for providing satellite altimetry data presented in Supporting Information S1. The *R/V Falkor* ship time was provided by a Schmidt Ocean Institute Grant to KLC and ARB. The AT37-12 research cruise was funded by the NSF OCE-1559042 and OCE-1559198 Grants. This work was funded by Simons Foundation Grant 622065, NSF Grants OCE-2138890 and OCE-2142998 to ARB, NSF Grants OCE-1923312 and OCE-2148468 to RJW, the MIT Ally of Nature Award, and the generous support of Dr. Bruce L. Heflinger. Additionally, DD was partially funded by an NSF Graduate Research Fellowship. Finally, we thank Babbin lab members and Adam Subhas for their support and comments on the manuscript and Rémi Buisson for his assistance in creating Figure 1.

- Chang, B. X., Devol, A. H., & Emerson, S. R. (2012). Fixed nitrogen loss from the eastern tropical North Pacific and Arabian Sea oxygen deficient zones determined from measurements of $N_2:Ar$. *Global Biogeochemical Cycles*, 26(3), GB3030. <https://doi.org/10.1029/2011GB004207>
- Chang, B. X., Rich, J. R., Jayakumar, A., Naik, H., Pratihary, A. K., Keil, R. G., et al. (2014). The effect of organic carbon on fixed nitrogen loss in the eastern tropical South Pacific and Arabian Sea oxygen deficient zones. *Limnology and Oceanography*, 59(4), 1267–1274. <https://doi.org/10.4319/llo.2014.59.4.1267>
- Codispoti, L. A., Brandes, J. A., Christensen, J. P., Devol, A. H., Naqvi, S. W. A., Paerl, H. W., & Yoshinari, T. (2001). The oceanic fixed nitrogen and nitrous oxide budgets: Moving targets as we enter the anthropocene? *Scientia Marina*, 65(S2), 85–105. <https://doi.org/10.3989/scimar.2001.65s285>
- Cram, J. A., Fuchsman, C. A., Duffy, M. E., Pretty, J. L., Lekanoff, R. M., Neibauer, J. A., et al. (2022). Slow particle remineralization, rather than suppressed disaggregation, drives efficient flux transfer through the Eastern Tropical North Pacific Oxygen Deficient Zone. *Global Biogeochemical Cycles*, 36(1), e2021GB007080. <https://doi.org/10.1029/2021GB007080>
- Dalsgaard, T., Stewart, F. J., Thamdrup, B., De Brabandere, L., Revsbech, N. P., Ulloa, O., et al. (2014). Oxygen at nanomolar levels reversibly suppresses process rates and gene expression in anammox and denitrification in the oxygen minimum zone off northern Chile. *MBio*, 5(6), e01966-14. <https://doi.org/10.1128/mBio.01966-14>
- Dalsgaard, T., Thamdrup, B., Farias, L., & Revsbech, N. P. (2012). Anammox and denitrification in the oxygen minimum zone of the eastern South Pacific. *Limnology and Oceanography*, 57(5), 1331–1346. <https://doi.org/10.4319/llo.2012.57.5.1331>
- D'Errico, J. (2022). inpaint_nans. MATLAB central file exchange. Retrieved from https://www.mathworks.com/matlabcentral/fileexchange/4551-inpaint_nans
- Deutsch, C., Gruber, N., Key, R. M., Sarmiento, J. L., & Ganachaud, A. (2001). Denitrification and N_2 fixation in the Pacific Ocean. *Global Biogeochemical Cycles*, 15(2), 483–506. <https://doi.org/10.1029/2000GB001291>
- Devol, A. H. (2003). Solution to a marine mystery. *Nature*, 422(6932), 575–576. <https://doi.org/10.1038/422575a>
- DeVries, T., Deutsch, C., Rafter, P. A., & Primeau, F. (2013). Marine denitrification rates determined from a global 3-D inverse model. *Biogeosciences*, 10(4), 2481–2496. <https://doi.org/10.5194/bg-10-2481-2013>
- Dickson, A. G., Sabine, C. L., & Christian, J. R. (2007). *Guide to best practices for ocean CO₂ measurements* (Report). North Pacific Marine Science Organization. Retrieved from <https://repository.oceanbestpractices.org/handle/11329/249>
- Evans, N., Boles, E., Kwiecinski, J. V., Mullen, S., Wolf, M., Devol, A. H., et al. (2020). The role of water masses in shaping the distribution of redox active compounds in the Eastern Tropical North Pacific oxygen deficient zone and influencing low oxygen concentrations in the eastern Pacific Ocean. *Limnology and Oceanography*, 65(8), 1688–1705. <https://doi.org/10.1002/lno.11412>
- Feely, R. A., Sabine, C. L., Lee, K., Millero, F. J., Lamb, M. F., Greeley, D., et al. (2002). In situ calcium carbonate dissolution in the Pacific Ocean. *Global Biogeochemical Cycles*, 16(4), 91–1–91-12. <https://doi.org/10.1029/2002GB001866>
- Firing, E., FilipeBarna, A., & Abernathy, R. (2021). TEOS-10/GSW-Python: V3.4.1.post0 (version v3.4.1.post0) [Dataset]. Zenodo. <https://doi.org/10.5281/zenodo.5214122>
- Fuchsman, C. A., Devol, A. H., Casciotti, K. L., Buchwald, C., Chang, B. X., & Horak, R. E. A. (2018). An N isotopic mass balance of the Eastern Tropical North Pacific oxygen deficient zone. *Deep Sea Research Part II: Topical Studies in Oceanography*, 156, 137–147. <https://doi.org/10.1016/j.dsr2.2017.12.013>
- Fuchsman, C. A., Devol, A. H., Saunders, J. K., McKay, C., & Rocap, G. (2017). Niche partitioning of the N cycling microbial community of an offshore oxygen deficient zone. *Frontiers in Microbiology*, 8, 2384. <https://doi.org/10.3389/fmicb.2017.02384>
- Fuchsman, C. A., Palevsky, H. I., Widner, B., Duffy, M., Carlson, M. C. G., Neibauer, J. A., et al. (2019). Cyanobacteria and cyanophage contributions to carbon and nitrogen cycling in an oligotrophic oxygen-deficient zone. *The ISME Journal*, 13(11), 2714–2726. <https://doi.org/10.1038/s41396-019-0452-6>
- Fuchsman, C. A., Paul, B., Staley, J. T., Yakushev, E. V., & Murray, J. W. (2019). Detection of transient denitrification during a high organic matter event in the Black Sea. *Global Biogeochemical Cycles*, 33(2), 143–162. <https://doi.org/10.1029/2018GB006032>
- Füssel, J., Lam, P., Lavik, G., Jensen, M. M., Holtappels, M., Günter, M., & Kuypers, M. M. (2012). Nitrite oxidation in the Namibian oxygen minimum zone. *The ISME Journal*, 6(6), 1200–1209. <https://doi.org/10.1038/ismej.2011.178>
- Ganesh, S., Bristow, L. A., Larsen, M., Sarode, N., Thamdrup, B., & Stewart, F. J. (2015). Size-fraction partitioning of community gene transcription and nitrogen metabolism in a marine oxygen minimum zone. *The ISME Journal*, 9(12), 2682–2696. <https://doi.org/10.1038/ismej.2015.44>
- García-Robledo, E., Padilla, C. C., Aldunate, M., Stewart, F. J., Ulloa, O., Paulmier, A., et al. (2017). Cryptic oxygen cycling in anoxic marine zones. *Proceedings of the National Academy of Sciences*, 114(31), 8319–8324. <https://doi.org/10.1073/pnas.1619844114>
- Gruber, N., & Sarmiento, J. L. (1997). Global patterns of marine nitrogen fixation and denitrification. *Global Biogeochemical Cycles*, 11(2), 235–266. <https://doi.org/10.1029/97GB00077>
- Hardisty, D. S., Horner, T. J., Evans, N., Moriyasu, R., Babbín, A. R., Wankel, S. D., et al. (2021). Limited iodate reduction in shipboard seawater incubations from the Eastern Tropical North Pacific oxygen deficient zone. *Earth and Planetary Science Letters*, 554, 116676. <https://doi.org/10.1016/j.epsl.2020.116676>
- Hernandez-Ayon, J. M., Paulmier, A., Garçon, V., Sudre, J., Montes, I., Chapa-Balcorta, C., et al. (2019). Dynamics of the carbonate system across the Peruvian oxygen minimum zone. *Frontiers in Marine Science*, 6, 617. <https://doi.org/10.3389/fmars.2019.00617>
- Huber, P. J. (1973). Robust regression: Asymptotics, conjectures and Monte Carlo. *Annals of Statistics*, 1(5), 799–821. <https://doi.org/10.1214/aos/1176342503>
- Humphreys, M., Pierrot, D., & van Heuven, S. (2020). PyCO2SYS: Marine carbonate system calculations in Python. Version 1.3. 0 [Dataset]. Zenodo. <https://zenodo.org/record/5176106%23.Y5FGQXZBw2w>
- Ji, Q., Babbín, A. R., Jayakumar, A., Oleynik, S., & Ward, B. B. (2015). Nitrous oxide production by nitrification and denitrification in the Eastern Tropical South Pacific oxygen minimum zone. *Geophysical Research Letters*, 42(24), 10755–10764. <https://doi.org/10.1002/2015GL066853>
- Jiang, L.-Q., Carter, B. R., Feely, R. A., Lauvset, S. K., & Olsen, A. (2019). Surface ocean pH and buffer capacity: Past, present and future. *Scientific Reports*, 9(1), 18624. <https://doi.org/10.1038/s41598-019-55039-4>
- Jørgensen, B. B. (1982). Mineralization of organic matter in the sea bed—The role of sulphate reduction. *Nature*, 296(5858), 643–645. <https://doi.org/10.1038/296643a0>
- Kalvelage, T., Lavik, G., Lam, P., Contreras, S., Arteaga, L., Löscher, C. R., et al. (2013). Nitrogen cycling driven by organic matter export in the South Pacific oxygen minimum zone. *Nature Geoscience*, 6(3), 228–234. <https://doi.org/10.1038/ngeo1739>
- Karstensen, J., Stramma, L., & Visbeck, M. (2008). Oxygen minimum zones in the eastern tropical Atlantic and Pacific oceans. *Progress in Oceanography*, 77(4), 331–350. <https://doi.org/10.1016/j.pocan.2007.05.009>
- Koeve, W., & Kähler, P. (2010). Heterotrophic denitrification vs. autotrophic anammox – Quantifying collateral effects on the oceanic carbon cycle. *Biogeosciences*, 7(8), 2327–2337. <https://doi.org/10.5194/bg-7-2327-2010>

- Kwiecinski, J. V., & Babbin, A. R. (2021). A high-resolution Atlas of the eastern tropical Pacific oxygen deficient zones. *Global Biogeochemical Cycles*, 35(12), e2021GB007001. <https://doi.org/10.1029/2021GB007001>
- Lam, P., Lavik, G., Jensen, M. M., van de Vossenberg, J., Schmid, M., Woebken, D., et al. (2009). Revising the nitrogen cycle in the Peruvian oxygen minimum zone. *Proceedings of the National Academy of Sciences*, 106(12), 4752–4757. <https://doi.org/10.1073/pnas.0812444106>
- Lauvset, S. K., Lange, N., Tanhua, T., Bittig, H. C., Olsen, A., Kozyr, A., et al. (2021). An updated version of the global interior ocean biogeochemical data product, GLODAPv2.2021. *Earth System Science Data*, 13(12), 5565–5589. <https://doi.org/10.5194/essd-13-5565-2021>
- Lee, K., Kim, T.-W., Byrne, R. H., Millero, F. J., Feely, R. A., & Liu, Y.-M. (2010). The universal ratio of boron to chlorinity for the North Pacific and North Atlantic oceans. *Geochimica et Cosmochimica Acta*, 74(6), 1801–1811. <https://doi.org/10.1016/j.gca.2009.12.027>
- Lipschultz, F., Zafiriou, O. C., & Ball, L. A. (1996). Seasonal fluctuations of nitrite concentrations in the deep oligotrophic ocean. *Deep Sea Research Part II: Topical Studies in Oceanography*, 43(2), 403–419. [https://doi.org/10.1016/0967-0645\(96\)00003-3](https://doi.org/10.1016/0967-0645(96)00003-3)
- Lomas, M. W., & Lipschultz, F. (2006). Forming the primary nitrite maximum: Nitrifiers or phytoplankton? *Limnology and Oceanography*, 51(5), 2453–2467. <https://doi.org/10.4319/lno.2006.51.5.2453>
- López-Sandoval, D. C., Lara-Lara, J. R., Lavín, M. F., Álvarez-Borrego, S., & Gaxiola-Castro, G. (2009). Primary productivity observations in the eastern tropical Pacific off Cabo Corrientes, Mexico. *Ciencias Marinas*, 35(2), 169–182. <https://doi.org/10.7773/cm.v35i2.1530>
- Lueker, T. J., Dickson, A. G., & Keeling, C. D. (2000). Ocean pCO₂ calculated from dissolved inorganic carbon, alkalinity, and equations for K₁ and K₂: Validation based on laboratory measurements of CO₂ in gas and seawater at equilibrium. *Marine Chemistry*, 70(1), 105–119. [https://doi.org/10.1016/S0304-4203\(00\)00022-0](https://doi.org/10.1016/S0304-4203(00)00022-0)
- Margolskee, A., Frenzel, H., Emerson, S., & Deutsch, C. (2019). Ventilation pathways for the North Pacific oxygen deficient zone. *Global Biogeochemical Cycles*, 33(7), 875–890. <https://doi.org/10.1029/2018GB006149>
- Millero, F. J. (2007). The marine inorganic carbon cycle. *Chemical Reviews*, 107(2), 308–341. <https://doi.org/10.1021/cr0503557>
- Milliman, J. D., Troy, P. J., Balch, W. M., Adams, A. K., Li, Y.-H., & Mackenzie, F. T. (1999). Biologically mediated dissolution of calcium carbonate above the chemical lysocline? *Deep Sea Research Part I: Oceanographic Research Papers*, 46(10), 1653–1669. [https://doi.org/10.1016/S0967-0637\(99\)00034-5](https://doi.org/10.1016/S0967-0637(99)00034-5)
- Moreno, A. R., Garcia, C. A., Larkin, A. A., Lee, J. A., Wang, W.-L., Moore, J. K., et al. (2020). Latitudinal gradient in the respiration quotient and the implications for ocean oxygen availability. *Proceedings of the National Academy of Sciences*, 117(37), 22866–22872. <https://doi.org/10.1073/pnas.2004986117>
- Moriyasu, R., Evans, N., Bolster, K. M., Hardisty, D. S., & Moffett, J. W. (2020). The distribution and redox speciation of iodine in the Eastern Tropical North Pacific Ocean. *Global Biogeochemical Cycles*, 34(2), e2019GB006302. <https://doi.org/10.1029/2019GB006302>
- Morrison, J. M., Codispoti, L. A., Gaurin, S., Jones, B., Manghnani, V., & Zheng, Z. (1998). Seasonal variation of hydrographic and nutrient fields during the US JGOFS Arabian Sea Process Study. *Deep Sea Research Part II: Topical Studies in Oceanography*, 45(10), 2053–2101. [https://doi.org/10.1016/S0967-0645\(98\)00063-0](https://doi.org/10.1016/S0967-0645(98)00063-0)
- Naqvi, S. W. A., Jayakumar, D. A., Narvekar, P. V., Naik, H., Sarma, V. V. S. S., D'Souza, W., et al. (2000). Increased marine production of N₂O due to intensifying anoxia on the Indian continental shelf. *Nature*, 408(6810), 346–349. <https://doi.org/10.1038/35042551>
- Olsen, A., Lange, N., Key, R. M., Tanhua, T., Álvarez, M., Becker, S., et al. (2019). GLODAPv2.2019 – An update of GLODAPv2. *Earth System Science Data*, 11(3), 1437–1461. <https://doi.org/10.5194/essd-11-1437-2019>
- Olsen, A., Lange, N., Key, R. M., Tanhua, T., Bittig, H. C., Kozyr, A., et al. (2020). An updated version of the global interior ocean biogeochemical data product, GLODAPv2.2020. *Earth System Science Data*, 12(4), 3653–3678. <https://doi.org/10.5194/essd-12-3653-2020>
- Pan, Y., Li, Y., Ma, Q., He, H., Wang, S., Sun, Z., et al. (2021). The role of Mg²⁺ in inhibiting CaCO₃ precipitation from seawater. *Marine Chemistry*, 237, 104036. <https://doi.org/10.1016/j.marchem.2021.104036>
- Paulmier, A., Kriest, I., & Oschlies, A. (2009). Stoichiometries of remineralisation and denitrification in global biogeochemical models. *Biogeosciences*, 6(5), 923–935. <https://doi.org/10.5194/bg-6-923-2009>
- Paulmier, A., & Ruiz-Pino, D. (2009). Oxygen minimum zones (OMZs) in the modern ocean. *Progress in Oceanography*, 80(3), 113–128. <https://doi.org/10.1016/j.pocean.2008.08.001>
- Paulmier, A., Ruiz-Pino, D., & Garçon, V. (2011). CO₂ maximum in the oxygen minimum zone (OMZ). *Biogeosciences*, 8(2), 239–252. <https://doi.org/10.5194/bg-8-239-2011>
- Pedregosa, F., Varoquaux, G., Gramfort, A., Michel, V., Thirion, B., Grisel, O., et al. (2011). Scikit-learn: Machine learning in Python. *Journal of Machine Learning Research*, 12, 2825–2830.
- Peng, X., Fuchsman, C. A., Jayakumar, A., Oleynik, S., Martens-Habbena, W., Devol, A. H., & Ward, B. B. (2015). Ammonia and nitrite oxidation in the Eastern Tropical North Pacific. *Global Biogeochemical Cycles*, 29(12), 2034–2049. <https://doi.org/10.1002/2015GB005278>
- Peng, X., Fuchsman, C. A., Jayakumar, A., Warner, M. J., Devol, A. H., & Ward, B. B. (2016). Revisiting nitrification in the Eastern Tropical South Pacific: A focus on controls. *Journal of Geophysical Research: Oceans*, 121(3), 1667–1684. <https://doi.org/10.1002/2015JC011455>
- Penn, J. L., Weber, T., Chang, B. X., & Deutsch, C. (2019). Microbial ecosystem dynamics drive fluctuating nitrogen loss in marine anoxic zones. *Proceedings of the National Academy of Sciences*, 116(15), 7220–7225. <https://doi.org/10.1073/pnas.1818014116>
- Pennington, J. T., Mahoney, K. L., Kuwahara, V. S., Kolber, D. D., Calienes, R., & Chavez, F. P. (2006). Primary production in the eastern tropical Pacific: A review. *Progress in Oceanography*, 69(2), 285–317. <https://doi.org/10.1016/j.pocean.2006.03.012>
- Perez, F. F., & Fraga, F. (1987). Association constant of fluoride and hydrogen ions in seawater. *Marine Chemistry*, 21(2), 161–168. [https://doi.org/10.1016/0304-4203\(87\)90036-3](https://doi.org/10.1016/0304-4203(87)90036-3)
- Peters, B. D., Babbin, A. R., Lettmann, K. A., Mordy, C. W., Ulloa, O., Ward, B. B., & Casciotti, K. L. (2016). Vertical modeling of the nitrogen cycle in the eastern tropical South Pacific oxygen deficient zone using high-resolution concentration and isotope measurements. *Global Biogeochemical Cycles*, 30(11), 1661–1681. <https://doi.org/10.1002/2016GB005415>
- Pitt, K. A., Welsh, D. T., & Condon, R. H. (2009). Influence of jellyfish blooms on carbon, nitrogen and phosphorus cycling and plankton production. *Hydrobiologia*, 616(1), 133–149. <https://doi.org/10.1007/s10750-008-9584-9>
- Raven, M. R., Keil, R. G., & Webb, S. M. (2021). Microbial sulfate reduction and organic sulfur formation in sinking marine particles. *Science*, 371(6525), 178–181. <https://doi.org/10.1126/science.abc6035>
- Ravishankara, A., Daniel, J. S., & Portmann, R. W. (2009). Nitrous oxide (N₂O): The dominant ozone-depleting substance emitted in the 21st century. *Science*, 326(5949), 123–125. <https://doi.org/10.1126/science.1176985>
- Redfield, A. C. (1958). The biological control of chemical factors in the environment. *American Scientist*, 46(3), 205–221.
- Revsbech, N. P., Larsen, L. H., Gundersen, J., Dalsgaard, T., Ulloa, O., & Thamdrup, B. (2009). Determination of ultra-low oxygen concentrations in oxygen minimum zones by the STOX sensor. *Limnology and Oceanography: Methods*, 7(5), 371–381. <https://doi.org/10.4319/lom.2009.7.371>
- Sasakawa, M., Tsunogai, U., Kameyama, S., Nakagawa, F., Nojiri, Y., & Tsuda, A. (2008). Carbon isotopic characterization for the origin of excess methane in subsurface seawater. *Journal of Geophysical Research*, 113(C3), C03012. <https://doi.org/10.1029/2007JC004217>

- Saunders, J. K., Fuchsman, C. A., McKay, C., & Rocap, G. (2019). Complete arsenic-based respiratory cycle in the marine microbial communities of pelagic oxygen-deficient zones. *Proceedings of the National Academy of Sciences*, *116*(20), 9925–9930. <https://doi.org/10.1073/pnas.1818349116>
- Schmale, O., Wäge, J., Mohrholz, V., Wasmund, N., Gräwe, U., Rehder, G., et al. (2018). The contribution of zooplankton to methane supersaturation in the oxygenated upper waters of the central Baltic Sea. *Limnology and Oceanography*, *63*(1), 412–430. <https://doi.org/10.1002/lno.10640>
- Stramma, L., Schmidtko, S., Levin, L. A., & Johnson, G. C. (2010). Ocean oxygen minima expansions and their biological impacts. *Deep Sea Research Part I: Oceanographic Research Papers*, *57*(4), 587–595. <https://doi.org/10.1016/j.dsr.2010.01.005>
- Strickland, J. D. H., & Parsons, T. R. (1972). A practical handbook of seawater analysis.
- Strous, M., Heijnen, J. J., Kuenen, J. G., & Jetten, M. S. M. (1998). The sequencing batch reactor as a powerful tool for the study of slowly growing anaerobic ammonium-oxidizing microorganisms. *Applied Microbiology and Biotechnology*, *50*(5), 589–596. <https://doi.org/10.1007/s002530051340>
- Subhas, A. V., Dong, S., Naviaux, J. D., Rollins, N. E., Ziveri, P., Gray, W., et al. (2022). Shallow calcium carbonate cycling in the North Pacific Ocean. *Global Biogeochemical Cycles*, *36*(5), e2022GB007388. <https://doi.org/10.1029/2022GB007388>
- Thamdrup, B., Dalsgaard, T., & Revsbech, N. P. (2012). Widespread functional anoxia in the oxygen minimum zone of the Eastern South Pacific. *Deep Sea Research Part I: Oceanographic Research Papers*, *65*, 36–45. <https://doi.org/10.1016/j.dsr.2012.03.001>
- Thamdrup, B., Steinsdóttir, H. G. R., Bertagnolli, A. D., Padilla, C. C., Patin, N. V., Garcia-Robledo, E., et al. (2019). Anaerobic methane oxidation is an important sink for methane in the ocean's largest oxygen minimum zone. *Limnology and Oceanography*, *64*(6), 2569–2585. <https://doi.org/10.1002/lno.11235>
- Tiano, L., Garcia-Robledo, E., Dalsgaard, T., Devol, A. H., Ward, B. B., Ulloa, O., et al. (2014). Oxygen distribution and aerobic respiration in the north and south eastern tropical Pacific oxygen minimum zones. *Deep Sea Research Part I: Oceanographic Research Papers*, *94*, 173–183. <https://doi.org/10.1016/j.dsr.2014.10.001>
- Tsimentzi, D., Wu, J., Deutsch, S., Nath, S., Rodriguez-R, L. M., Burns, A. S., et al. (2016). SAR11 bacteria linked to ocean anoxia and nitrogen loss. *Nature*, *536*(7615), 179–183. <https://doi.org/10.1038/nature19068>
- Van Heuven, S., Pierrot, D., Rae, J., Lewis, E., & Wallace, D. (2011). *MATLAB Program developed for CO₂ system calculations, ORNL/CDIAC-105b* (p. 530). Carbon Dioxide Information Analysis Center, Oak Ridge National Laboratory, US Department of Energy.
- Ventura, M. (2006). Linking biochemical and elemental composition in freshwater and marine crustacean zooplankton. *Marine Ecology Progress Series*, *327*, 233–246. <https://doi.org/10.3354/meps327233>
- Virtanen, P., Gommers, R., Oliphant, T. E., Haberland, M., Reddy, T., Cournapeau, D., et al. (2020). SciPy 1.0: Fundamental Algorithms for scientific computing in Python. *Nature Methods*, *17*(3), 261–272. <https://doi.org/10.1038/s41592-019-0686-2>
- Ward, B. B. (2013). How nitrogen is lost. *Science*, *341*(6144), 352–353. <https://doi.org/10.1126/science.1240314>
- Ward, B. B., Devol, A. H., Rich, J. J., Chang, B. X., Bulow, S. E., Naik, H., et al. (2009). Denitrification as the dominant nitrogen loss process in the Arabian Sea. *Nature*, *461*(7260), 78–81. <https://doi.org/10.1038/nature08276>
- Widner, B., Fuchsman, C. A., Chang, B. X., Rocap, G., & Mulholland, M. R. (2018). Utilization of urea and cyanate in waters overlying and within the eastern tropical north Pacific oxygen deficient zone. *FEMS Microbiology Ecology*, *94*(10), fiy138. <https://doi.org/10.1093/femsec/fiy138>
- Woosley, R. J. (2021). Long-term stability and storage of meta-cresol purple solutions for seawater pH measurements. *Limnology and Oceanography: Methods*, *19*(12), 810–817. <https://doi.org/10.1002/lom3.10462>
- Woosley, R. J., Millero, F. J., & Grosell, M. (2012). The solubility of fish-produced high magnesium calcite in seawater. *Journal of Geophysical Research*, *117*(C4). <https://doi.org/10.1029/2011JC007599>
- Zakem, E. J., Al-Haj, A., Church, M. J., van Dijken, G. L., Dutkiewicz, S., Foster, S. Q., et al. (2018). Ecological control of nitrite in the upper ocean. *Nature Communications*, *9*(1), 1206. <https://doi.org/10.1038/s41467-018-03553-w>
- Zakem, E. J., & Follows, M. J. (2017). A theoretical basis for a nanomolar critical oxygen concentration. *Limnology and Oceanography*, *62*(2), 795–805. <https://doi.org/10.1002/lno.10461>
- Zhang, Y., Qin, W., Hou, L., Zakem, E. J., Wan, X., Zhao, Z., et al. (2020). Nitrifier adaptation to low energy flux controls inventory of reduced nitrogen in the dark ocean. *Proceedings of the National Academy of Sciences*, *117*(9), 4823–4830. <https://doi.org/10.1073/pnas.1912367117>